Chapter 4

Wave Propagation in Elastic Medium

Buddhism statue at Longmen (龍門) in Luoyang (洛陽), China.
This was a place where rich people in the capital city of Luoyang donated statues for dead people. Descriptions on the life of the dead people were carved on rock and have been considered as the best calligraphy .

4.1 Earthquake Waves: S Wave

S wave (Secondary wave) is a propagation of shear deformation that arrives at earthquake observation stations after (second to) the Primary body wave (P wave, see Sect. 4.2). Since S wave generates a significant magnitude of horizontal motion at the ground surface, it is considered to be the most important cause of seismic damage.

Figure 4.1 illustrates the derivation of S-wave propagation equation for which a study is made of equation of motion of a small soil element in an semi-infinite level and elastic ground

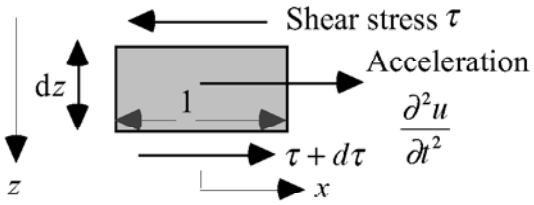

Fig. 4.1 Derivation of S-wave propagation equation

$$\rho \frac{\partial^2 u}{\partial t^2} = \frac{\partial \tau}{\partial z}, \qquad (4.1)$$

where u is the horizontal displacement, and ρ stands for the mass density of soil (1.5–2 times that of water in most situations), while τ is the shear stress in a horizontal plane at the top and bottom of the concerned soil element. Lateral normal stresses on the left and right sides of the element are not included in the equation. This is because the assumption of a homogeneous level ground subjected to horizontal shaking makes everything constant in the x direction and, consequently, the normal stresses on two sides are equal to and cancel each other.

Another assumption of linear elasticity correlates shear stress with shear strain and displacement

$$\tau = G \times (\text{shear strain}) = G \frac{\partial u}{\partial z}, \qquad (4.2)$$

in which shear modulus of soil is designated by G. By substituting (4.2) in (4.1) and using a new notation of $V_s = \sqrt{G/\rho}$,

$$\frac{\partial^2 u}{\partial t^2} = \frac{G}{\rho} \frac{\partial^2 u}{\partial z^2} = V_s^2 \frac{\partial^2 u}{\partial z^2}. \qquad (4.3)$$

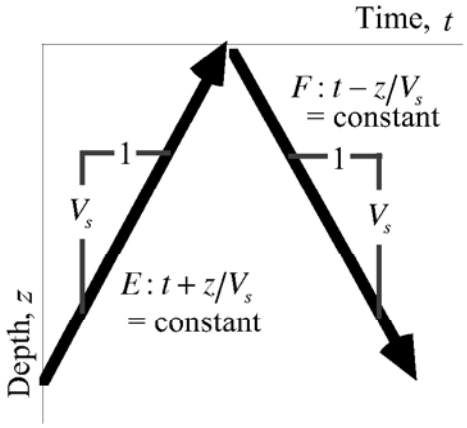

Fig. 4.2 Rate of wave propagation

The general solution of (4.3) is given by

$$u(t,z) = E(t + z/V_s) + F(t - z/V_s), \qquad (4.4)$$

in which E and F are arbitrary functions of $t+z/V_s$ and $t-z/V_s$, respectively. They have to be arbitrary because the time history of earthquake motions are irregular.

Figure 4.2 shows that the motions represented by E and F travel upwards or downwards at the rate of V_s per second. For example, suppose that $E = 1.2345$ when $t+z/V_s = 2.00$. There are many combinations of t and z for which $t+z/V_s = 2.00$. The only requirement for $E = 1.2345$ is that z decreases by V_s when t increases by 1. Thus, the phenomenon of E = *1.2345* moves upwards at the rate of V_s per second. Accordingly the horizontal shaking accounted for by E function travels upwards at the speed of V_s. Similarly, the F component of shaking propagates downwards at the rate of V_s. Hence, V_s is called the S-wave propagation velocity.

Thus, the horizontal shaking was decomposed into two parts: upward and downward propagations. Propagating inside a solid medium, S wave is one of what are called body waves. Typical V_s values are, approximately, 100 m/s for very soft soils, 300 m/s for stiff soils, and 3,000 m/s for hard intact rocks.

4.2 Earthquake Waves : P Wave

In addition to the S wave in Sect. 4.1, another kind of body wave that propagates in a homogeneous medium is called the P wave. P wave is a propagation of compression and extension (variation of pressure and volume change). Typical example of P wave is a propagation of sound, see Fig. 4.3.

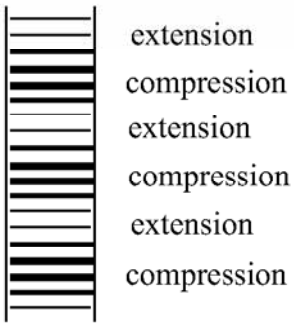

Fig. 4.3 Propagation of volume change in P wave propagation

The rate of P wave propagation is given by

$$V_{\mathrm{p}} = \sqrt{\frac{E(1-\nu)}{\rho(1-2\nu)(1+\nu)}}, \qquad (4.5)$$

where E is the modulus of elasticity and ν the Poisson ratio. Note that the Poisson ratio is equal to 0.5 in an incompressible material and makes V_{p} infinite.

It is a common practice in geophysical exploration that P wave is generated artificially by any impact or explosion so that its rate of propagation, V_{p}, may be measured. The obtained V_{p} value is substituted in (4.5) to back-calculate the value of E while the Poisson ratio is assumed to be more or less 0.25–0.3. It is noteworthy that this technique of subsurface exploration is useful for very stiff soil and rock. When this technology is conducted in soft soil of an alluvial plane where the ground water table is high, the measured V_{p} is often 1,400–1,500 m/s. Since the pore of soil is saturated with water and the modulus of compressibility of water is greater than that of soft soil skeleton, the measured V_{p} is the velocity of sound propagation in water without much correlation with the engineering nature of soil. In contrast, the P wave velocity, V_{p}, is, for example, 5,000 m/s in an intact rock mass.

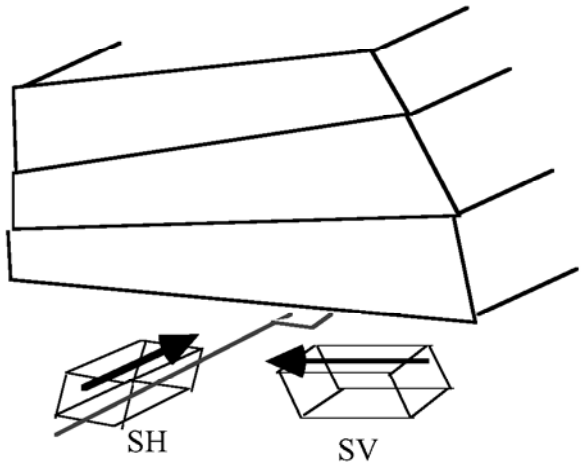

Fig. 4.4 Difference of SH and SV waves

There is an interaction between P and S waves. Figure 4.4 illustrates two kinds of S waves. For SH, the direction of soil particle motion is antiplane and perpendicular to the cross section of subsoil, while SV moves soil particles inside the plane. After SH wave arrives at the boundary of two different soils, the motion is still SH, although the direction of wave propagation may change (refraction 屈折 into the next layer and reflection 反射 back into the first layer) in accordance with the nature of soil (Fig. 4.5a). On the contrary, SV wave upon arrival at a boundary generates both P and SV waves in refracted and reflected phases as well (Fig. 4.5b). Because of the simplicity, most seismic risk analyses of regions and municipalities assume SH waves assuming horizontally layered ground. On the contrary, dynamic response analyses on important structures (foundations, dams, etc.) are conducted on two-dimensional cross sections and hence work on SV (not SH) waves.

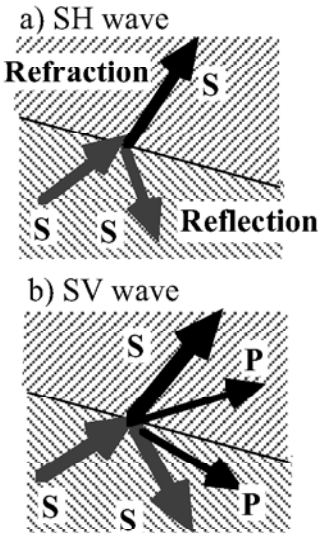

Fig. 4.5 Refraction and reflection of S waves at interface

An earthquake source generates both P and S waves simultaneously. At a focal distance of L, they arrive at different times because of different propagation velocities. The difference in arrival time is given by

$$\Delta T = \frac{L}{V_s} - \frac{L}{V_p}. \qquad (4.6)$$

This formula is used to assess the distance to the seismic source, L, by using the recorded time difference, ΔT. For wave propagation in earth crust, V_p and V_s in intact rock mass are relevant, $V_p = 5$ km/s and $V_s = 3$ km/s. If L from three observation points are known, it is possible to determine the location of the wave source.

Hard rock has V_p of typically 5,000 m/s. In soft water-saturated soil, P wave propagation in pore water is predominant. Hence, V_p in such a soil condition is similar to the velocity of sound in water. For example, the sound velocity in water is 1,483 m/s at 20 °C and 1,433 m/s at 15 °C. The sound velocity in air is 343.5 m/s at 20 °C.

4.3 Idealization of Vertical Wave Propagation

It is common that a (design) earthquake occurs at a distance of tens or hundreds of kilometers awayfrom the site of concern while the depth of fault rupture is again tens of kilometers. Hence, the source of earthquake wave propagation is not below the site to be studied, see Fig. 4.6. Therefore, the idea of vertical wave propagation as discussed in Sect. 4.1 appears to be inappropriate.

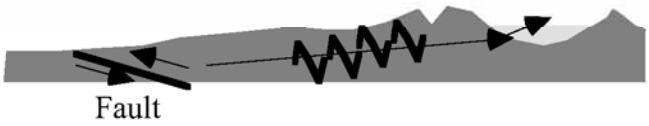

Fig. 4.6 Geometrical relationship between earthquake source and site of interest

Actually, the direction of wave propagation in an alluvial soft deposit should be studied in a more detailed scale (Fig. 4.7). For instance, the propagation velocity of S wave (V_s) is a function of shear rigidity, G

$$V_s = \sqrt{G/\rho}\,. \qquad (4.7)$$

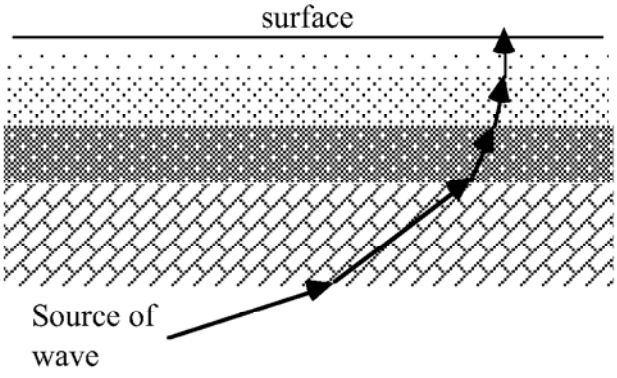

Fig. 4.7 Wave path in alluvium

Since G of geomaterials is smaller at shallower depth, V_s decreases as well towards the ground surface. Hence, Snell's law of wave refraction at an interface of two different wave velocities states that the wave propagation should change its direction to be more vertical, in general, as the ground surface is approached.

From Snell's law in Fig. 4.8, using a proportionality parameter of α,

$$\sin i = \frac{\mathrm{d}x}{\sqrt{\mathrm{d}x^2 + \mathrm{d}z^2}} = \alpha \times V_s \le 1 \quad \text{or}$$

$$\frac{\mathrm{d}x}{\mathrm{d}z} = \frac{\alpha^2 V_s^2}{1 - \alpha^2 V_s^2}. \qquad (4.8)$$

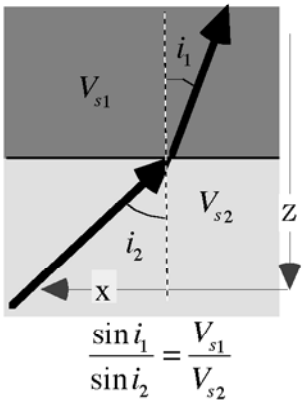

Fig. 4.8 Snell's law of wave refraction at interface

By assuming $\alpha^2 V_s^2 = \alpha^2 G/\rho = z^n$ in which n accounts for the effects of depth (or effective stress) on G,

$$\frac{\mathrm{d}x}{\mathrm{d}z} = \frac{z^n}{1 - z^n} = -1 + \frac{1}{1 - z^n}. \qquad (4.9)$$

Figure 4.9 illustrates the integration of (4.9) that governs the change of direction of wave propagation. "n = 1" was employed only for easy calculation; $n < 1$ is more likely in reality. Note that Fig. 4.9 assumes a continuous variation of V_s with depth, while V_s in reality changes discontinuously at interfaces of materials of different geological ages. One of the important discontinuity occurs between alluvial and pleistocene deposits.

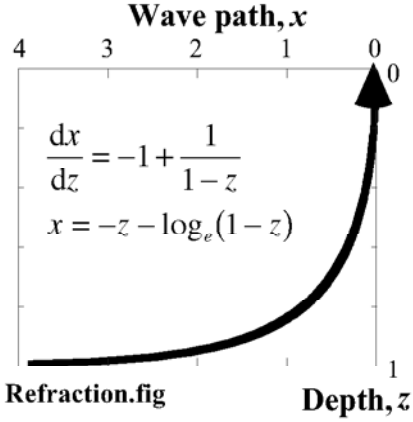

Fig. 4.9 Example calculation of change of wave propagation direction due to continuous variation of G with depth

4.4 Vertical Propagation of "S" Wave in Level Ground

The most important type of earthquake shaking is conventionally, and most probably in future as well, the S wave that produces a ground motion in the horizontal direction. This direction of motion is substantially efficient in causing damage to surface structures.

As was already shown in Fig. 4.9, it is reasonable at a shallow depth to assume a vertical propagation of S wave. See Fig. 4.10 in this Section.

In what follows, the horizontal displacement of a soil grain is denoted by u. The equation of wave propagation is given by

$$\frac{\partial^2 u}{\partial t^2} = V_s^2 \frac{\partial^2 u}{\partial z^2}, \qquad (4.10)$$

in which $V_s = \sqrt{G/\rho}$.

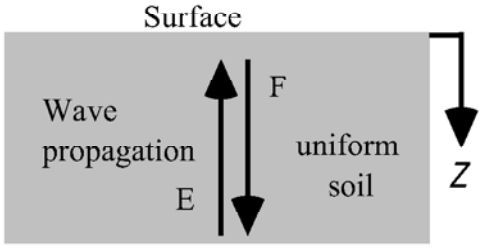

Fig. 4.10 Vertical propagation of S wave in level subsoil

A harmonic solution (sinusoidal solution) of (4.10) is derived by assuming that u varies with time in accordance with $\sin(\omega t)$ and $\cos(\omega t)$ functions. The symbol of ω denotes a circular frequency of shaking (円振動数), which is equivalent with a frequency of $\omega/2\pi$. It is, however, more efficient to use in this section a complex exponential function,

$$u(z,t) = A(z)\ \exp(\mathrm{i}\omega t), \qquad (4.11)$$

where $i = \sqrt{-1}$ and A is an unknown function of z. In case this complex expression is not easy, it is acceptable for a reader to go to Sect. 4.5. In that section, it will be demonstrated that expressions in terms of complex number and real number are equivalent but that the complex number can save time. Note that the real and complex parts of the exponential function in (4.11) are cos and sin functions,

$$\exp(i\omega t) = \cos(\omega t) + i\ \sin(\omega t), \qquad (4.12)$$

By substituting (4.11) in (4.10),

$$\frac{\mathrm{d}^2 A}{\mathrm{d}z^2} = -\left(\frac{\omega}{V_s}\right)^2 A \quad \text{and, accordingly,} \quad A = E\ \exp\left(\frac{\mathrm{i}\omega z}{V_s}\right) + F\ \exp\left(-\frac{\mathrm{i}\omega z}{V_s}\right), \qquad (4.13)$$

where E and F are constant parameters that are determined by boundary conditions. The solution for "u" is finally derived as

$$u(z,t) = \left\{A = E\ \exp\left(\frac{\mathrm{i}\omega z}{V_s}\right) + F\ \exp\left(-\frac{\mathrm{i}\omega z}{V_s}\right)\right\}\exp(\mathrm{i}\omega t) = E\ \exp\left\{\mathrm{i}\omega\left(t + \frac{z}{V_s}\right)\right\} + F\ \exp\left\{\mathrm{i}\omega\left(t - \frac{z}{V_s}\right)\right\}. \qquad (4.14)$$

The E and F terms in (4.14) stand for an upward and downward wave propagations, respectively. See Fig. 4.10. Equation (4.14) states that "u" varies with $\exp(\mathrm{i}\omega t)$ in terms of time. Hence, when ωt increases by 2π, the value of "u" comes back to the original value. Hence, $2\pi/\omega$ is the period of shaking. Similarly, "u" varies with $\exp(\mathrm{i}\omega z/V_s)$ in terms of depth, and $2\pi V_s/\omega$ stands for the wave length. Further, ω/V_s is sometimes called the wave number. A further study will continue in Sect. 6.7.

Although a harmonic motion is not a reality, it is still very important in practice. This is because the real irregular ground motion can be divided into harmonic components of various frequencies, Fourier series (Sect. 9.11). Each component has a different intensity and it is further amplified to a different extent in the surface alluvium. This is called the local soil effect.

4.5 Solution of S-Wave Propagation in Real Numbers

The equation of S-wave propagation is given by

$$\frac{\partial^2 u}{\partial t^2} = V_s^2 \frac{\partial^2 u}{\partial z^2}. \qquad (4.15)$$

By assuming its harmonic solution with real numbers,

$$u(z,t) = A(z)\sin(\omega t). \qquad (4.16)$$

By substituting (4.16) in (4.15),

$$-\omega^2 A \sin\omega t = V_s^2 \frac{\mathrm{d}^2 A}{\mathrm{d}z^2}\sin\omega t. \qquad (4.17)$$

Consequently,

$$\frac{\mathrm{d}^2 A}{\mathrm{d}z^2} = -\left(\frac{\omega}{V_s}\right)^2 A \qquad (4.18)$$

whose solution is given by

$$A = A_1 \sin\frac{\omega z}{V_s} + A_2 \cos\frac{\omega z}{V_s}, \qquad (4.19)$$

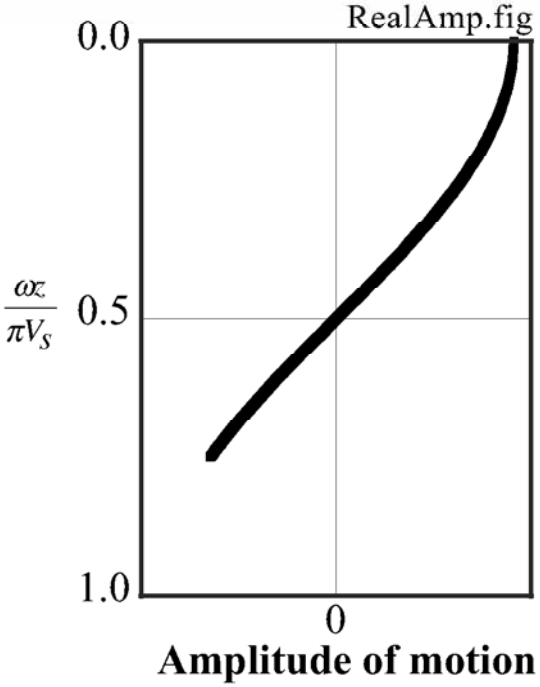

Fig. 4.11 Variation of shaking amplitude in vertical direction

in which A_1 and A_2 are constant parameters to be determined by boundary conditions. Accordingly,

$$u(z,t) = \frac{A_1}{2}\left[-\cos\left\{\omega\left(\frac{z}{V_s}+t\right)\right\} + \cos\left\{\omega\left(\frac{z}{V_s}-t\right)\right\}\right] + \frac{A_2}{2}\left[\sin\left\{\omega\left(\frac{z}{V_s}+t\right)\right\} - \sin\left\{\omega\left(\frac{z}{V_s}-t\right)\right\}\right]. \qquad (4.20)$$

Note thus that this solution consists of the upward $\left(\frac{z}{V_s}+t\right)$ and downward $\left(\frac{z}{V_s}-t\right)$ propagations of motion.

Since the ground surface is an interface of soil with air or water in which shear stress is zero, the boundary condition at the ground surface ($z = 0$) specifies

$$\tau = G \times (\text{shear strain}) = G\frac{\partial u}{\partial z} = 0 \text{ or } \quad \frac{\partial u}{\partial z} = 0 \text{ and } \frac{\mathrm{d}A}{\mathrm{d}z} = 0. \qquad (4.21)$$

Accordingly, $A_1 = 0$

$$A(z) = A_2 \cos\frac{\omega z}{V_s} \qquad \text{and} \qquad u(z,t) = A_2 \cos\frac{\omega z}{V_s}\sin\omega t. \qquad (4.22)$$

Figure 4.11 illustrates the variation of the amplitude of motion, $A(z)$, in the vertical direction. Note that the sign of "A" changes below $\omega z/V_s = \pi/2$. This implies that the ground surface and soil below some depth move in opposite directions. It is interesting that there is a special depth at which the amplitude is zero.

The simplest type of amplification of motion is defined by the ratio of motion at the surface and at the

base (base stiff soil or rock) at $z = H$;

$$\mathrm{Amp}(E+F) \equiv \frac{\text{Amplitude of motion at surface}}{\text{Amplitude of motion at base}} = \frac{|A(z=0)|}{|A(z=H)|} = \frac{1}{\left|\cos\dfrac{\omega H}{V_s}\right|}. \qquad (4.23)$$

Figure 4.12 demonstrates the variation of amplification with $\omega H/V_s$. The amplification thus varies with the frequency of motion (frequency = $\omega/2\pi$) and the thickness of surface soil (H). The maximum value of amplification (resonance) occurs when $\omega H/V_s = \left(n - \dfrac{1}{2}\right) \times \pi$ in which n=1,2,3,$\cdots$. When n = 1/2 in particular,

$$\omega H/V_s = \frac{\pi}{2}, \quad \omega = \frac{\pi V_s}{2H}, \text{ frequency} = \frac{\omega}{2\pi} = \frac{V_s}{4H}, \text{ and}$$
$$\text{the period of motion} = \frac{1}{\text{frequency}} = \frac{4H_s}{V_s}, \qquad (4.24)$$

which is very important in seismic microzonation. The amplification means that the surface motion is Amp(E+F) times greater than the motion at the base.

Although Fig. 4.12 suggests an infinite value of amplification at resonance, the reality does not cause infinite intensity of surface motion upon (small) motion at the base. Real soil and ground have many kinds of energy loss and does not enable such a strong motion; see Sect. 9.6 and Chap 10.

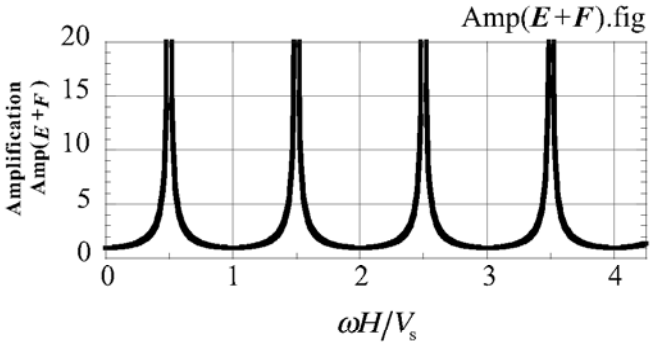

Fig. 4.12 Amplification of motion in ideally linearly elastic ground

4.6 Exercise No. 1 on Amplification of Ground Motion

1. Take the real parts of (4.14) in Sect. 4.4. Determine the relationship between two unknown parameters, E and F, by using a boundary condition at the ground surface. Do not forget that "E" and "F" are complex numbers.
   Boundary condition: Since the ground surface (z=0) is a free surface, there is no shear stress, $G\frac{\partial u}{\partial z} = 0$. Since $G \neq 0$, $\frac{\partial u}{\partial z} = 0$.
2. Remove "F" from concerned formulae by using the relationship derived in [1]. Then, plot the relationship between the amplitude of shaking displacement "u" and the depth. Use high and low values of frequency (high and low values of ω).
3. Calculate the amplification factor which is the ratio of the amplitudes of shaking motion "u" at the surface and at the bottom of the surface soil ($z = H$).
4. Calculate the amplification similarly for a situation where there is a rigid mass of "M" per unit area at the ground surface.

For answers, see the end of this book.

The Rayleigh wave travels along the ground surface (surface wave). It does not propagate into the earth. The displacements, u and w in Fig. 4.13, are analytically given in complex numbers

$$u = \mathrm{i}AN\left[-\exp\left\{-\frac{q}{N}(zN)\right\} + \frac{2\frac{q}{N}\frac{s}{N}}{\frac{s^2}{N^2}+1}\exp\left\{-\frac{s}{N}(zN)\right\}\right]\exp\{\mathrm{i}(\omega t)Nx\}$$

$$w = \mathrm{i}AN\left[\frac{2\frac{q}{N}}{\frac{s^2}{N^2}+1}\exp\left\{-\frac{s}{N}(zN)\right\} - \frac{q}{N}\exp\left\{-\frac{q}{N}(zN)\right\}\right]\exp\{\mathrm{i}(\omega t)Nx\},$$

in which $\mathrm{i} = \sqrt{-1}$, A is constant, N the wave number with the wave length = 2π/N, and ω the circular frequency. Moreover,

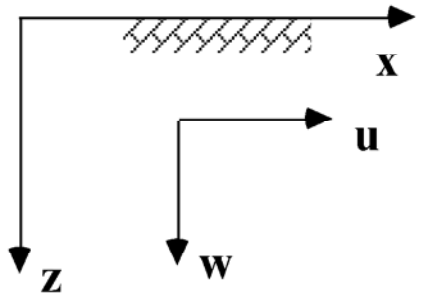

Fig. 4.13 Positive direction of coordinates and displacements

$$q = \sqrt{N^2 - \omega^2/V_\mathrm{p}^2} \quad \text{and} \quad s = \sqrt{N^2 - \omega^2/V_\mathrm{s}^2}$$

The wave number, N, is calculated by $N = \omega/V_\mathrm{s}K$ in which K is a solution of

$$K^6 - 8K^4 + \left(24 - 8\frac{1-2\nu}{1-\nu}\right)K^2 - \frac{8}{1-\nu} = 0$$

and is given as

Poisson ratio ν	0.0	0.1	0.2	0.3	0.333	0.4	0.5
$K = V_\mathrm{r}/V_\mathrm{s}$	0.874	0.893	0.911	0.927	0.933	0.942	0.955

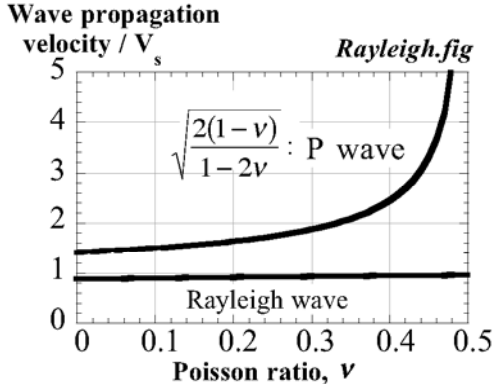

Fig. 4.14 Wave propagation velocities

The velocity of Rayleigh wave, V_r, is slightly smaller than V_s, see Fig. 4.14. Figure 4.15 illustrates the orbit of particle movement near the surface (z=0). When the wave propagates towards the right, the particle rotates in a counterclockwise direction. Bolt (1993) drew a good illustration of the material movement in Rayleigh wave. The direction of the particle movement is reversed below some depth to be clockwise.

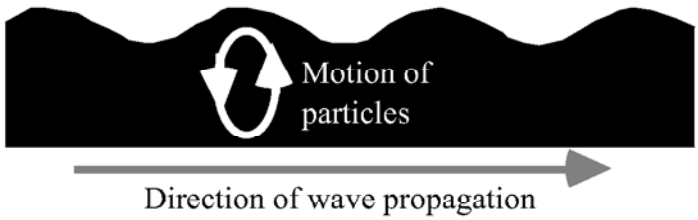

Fig. 4.15 Form of Rayleigh-wave motion in elastic medium

When the subsoil is composed of soil layers that have different shear wave velocities (V_s), the propagation velocity of Rayleigh wave is variable. Rayleigh wave of longer wave length (long period) is affected by nature of soils at greater depth where V_s is higher, and its propagation velocity is greater. On the contrary, Rayleigh wave of shorter wave length (high frequency) is controlled by soils at shallower elevation, and its propagation velocity is slower. This nature is applied to subsurface soil investigation in which the propagation velocity of many Rayleigh-wave components are measured and shear modulus of soils at corresponding depth is determined.

Seismologists are interested in Rayleigh wave traveling along the earth´s perimeter. However, that wave causes a very small intensity of ground shaking without affecting engineering facilities. Earthquake geotechnical engineering is interested in Rayleigh waves that are generated when the incident P and S

waves hit the surface irregularity and are reflected. A surface wave seems to decay quickly as it travels along the surface of soft deposits. It cannot reach a far distance. This is because the soft soil has a hysteresis stress–strain loop and the wave energy decays quickly during the propagation.

Application of Rayleigh wave to site investigation: Artificially generate Rayleigh wave (Sect. 4.9) and measure its propagation velocity V_r, at surface. Since $V_r \cong V_s = \sqrt{G/\rho}$, "$G$" of soil is obtained. "$\rho$" is typically 1.8–2.0 ton/m^3.

4.8 Earthquake Waves : Love Wave

There is another type of surface wave that is called Love wave. This wave occurs when an elastic halfspace is overlain by a softer surface layer (Fig. 4.16). Harmonic solution (sinusoidal function) is given by

$$u_1 = \{A\ \exp(is_1 z) + B\ \exp(-is_1 z)\}\exp(-iqy)\exp(i\omega t)$$
$$u_2 = C\ \exp(-is_2 z)\exp(-iqy)\exp(i\omega t),$$

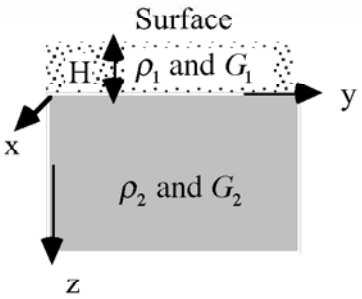

Fig. 4.16 Coordinates in Love-wave theory

where u_1 and u_1 stand for displacement in x direction in the upper and lower layers, respectively. A, B, and C are constants. Furthermore, ω is the circular frequency, and

$$s_1 = \sqrt{k_1^2 - q^2},\ k_1 = \omega / V_{s1},\ V_{s1} = \sqrt{G_1/\rho}$$
$$s_2 = \sqrt{k_2^2 - q^2},\ k_2 = \omega / V_{s2},\ V_{s2} = \sqrt{G_2/\rho}$$

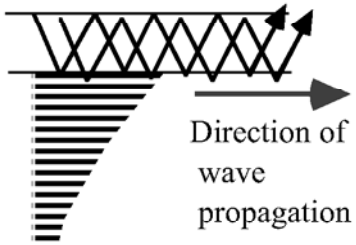

Fig. 4.17 Superimposed SH wave propagation

Since the particle motion is oriented in the x direction, Love wave is a type of SH wave. The above solution means that an upward and downward propagation of SH waves are superimposed (重複) in the upper layer; both propagating in y direction as well, whilst the lower layer has a horizontal propagation of a single SH wave (Fig. 4.17).

Figure 4.18 illustrates a view of ground deformation. The surface layer is sheared in both y and z directions. Bolt (1993) made a good illustration of particle movement in Love wave. Being SH wave, Love wave does not have a volume change.

A, B, and C parameters are determined by considering (1) shear stress = 0 at the ground surface ($z=-H$), and (2) both stress and displacement are continuous at the interface ($z=0$). The velocity of Love wave velocity, V_L, is given by

$$V_L = q/a = V_{s1}\sqrt{1 + s_1^2/q^2}\ .$$

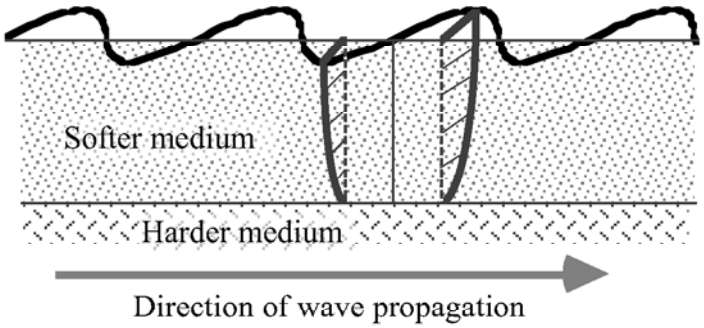

Fig. 4.18 Conceptual view of ground deformation in Love wave

When the wave length seen along the surface, $L=2p/q$, varies, q value changes as well and V_L changes

High frequency $\rightarrow$short L $\rightarrow$ V_L approaches V_{s1} and Low frequency $\rightarrow$long L $\rightarrow$ V_L approaches V_{s2}.

Thus, the wave propagation velocity of Love wave depends on the frequency. This fact makes dispersion and group velocity (U, 群速度). Vibration of different frequency propagates at different U. The principle lying behind this is similar to beeping (うなり).

$$\mathrm{d}(\omega t - qy)/\mathrm{d}q = 0 \qquad \therefore t(\mathrm{d}\omega/\mathrm{d}q) - y = 0 \qquad U = y/t = \mathrm{d}\omega/\mathrm{d}q = \mathrm{d}(V_L q)/\mathrm{d}q$$
$$\therefore U = V_L + q(\mathrm{d}V_L/\mathrm{d}q) = V_L - L(\mathrm{d}V_L/\mathrm{d}L).$$

4.9 Response of Elastic Ground to Surface Excitation

Figure 4.19 illustrates an elastic halfspace that is excited by a linear vertical loading. Solving the ground response under this situation is called Lamb´s problem. For details, see Båth (1968).

The solution of Lamb´s problem shows that the ground response to this linear loading consists of three components:

P wave : decays with distance
S wave : decays with distance
Rayleigh wave : no decay

The first two are body waves and propagates into the infinite body of ground. Therefore, they become weaker (decay) as they travel farther. In contrast, the surface wave (Rayleigh wave) maintains its amplitude to the infinity, because it travels along the surface.

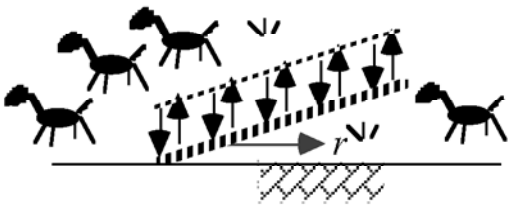

Fig. 4.19 Level ground excited by linear wave source at surface

When the surface loading is applied at a point (Fig. 4.20), all the three components of motion decay with distance. Table 4.1 reveals the rate of decay with the distance.

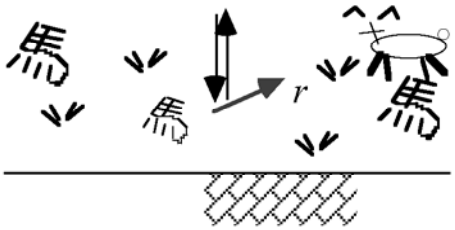

Fig. 4.20 Level ground excited by point wave source

Table 4.1 Decrease of wave amplitude at surface with distance from the source (geometrical damping)

Source	Rayleigh	P	S
Line	1	$r^{-3/2}$	$r^{-3/2}$
Point	$r^{-1/2}$	r^{-2}	r^{-2}

r: surface distance from source

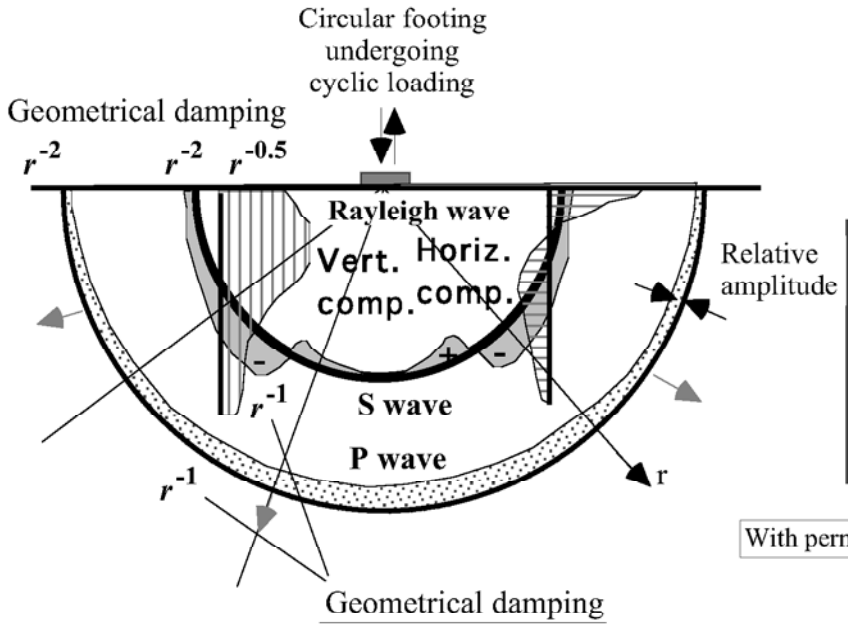

Shear window is the direction in which S-wave energy is concentrated.

Relative amplitude

Wave type	Percent of total energy
Rayleigh	67
Shear	26
Compression	7

With permission of ASCE

Fig. 4.21 Distribution of displacement waves from a circular footing on a homogeneous, isotropic, elastic halfspace (after Woods, 1968)

Figure 4.21 indicates the variation of energy and wave type with the direction of propagation. Under a circular oscillating footing, similar to a point loading, the energy of P wave (compression wave) is more important in the vertical direction, S wave is important in the inclined directions, and Rayleigh wave is significant near the surface.

4.10 Wave Transmission and Reflection at Interface

Study is made of SH wave propagation across an interface of two elastic layers. An infinite medium is assumed here (Fig. 4.22), and attention is focussed on transmission and reflection at the interface. Being denoted as "*a*" and "b", those two layers are of different impedance. An incident wave (入射波 E_b) arrives from the bottom and, at the interface, are partially transmitted into the next layer (透過波 E_a), while partially reflected back (反射波 F_b). Note that discussion in this section assumes infinite thickness of the upper layer without surface.

The displacement, u, and shear stress, τ, under harmonic excitation are given by

$$u_a = E_a \exp\left\{i\omega\left(t + z/V_{sa}\right)\right\} \text{ and}$$

$$\tau_a = G_a \frac{\partial u_a}{\partial z} = i\omega\rho_a V_{sa} E_a \exp\left\{i\omega\left(t + z/V_{sa}\right)\right\} \text{ in layer "a"}$$

$$u_b = E_b \exp\left\{i\omega\left(t + z/V_{sb}\right)\right\} + F_b \exp\left\{i\omega\left(t - z/V_{sb}\right)\right\} \text{ and}$$

$$\tau_a = i\omega\rho_b V_{sb}\left[E_b \exp\left\{i\omega\left(t + z/V_{sb}\right)\right\} - F_b \exp\left\{i\omega\left(t - z/V_{sb}\right)\right\}\right] \text{ in layer "b".}$$

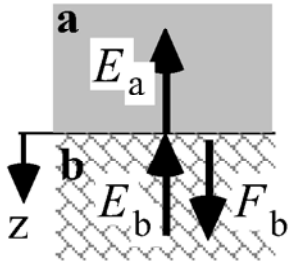

Fig. 4.22 Definition of incident and reflected waves near layer interface

Because of the continuity of displacement and shear stress at the interface (z=0),

$$\begin{cases} E_a = E_b + F_b \\ R \times E_a = E_b - F_b \end{cases} \text{ in which } R = \frac{\rho_a V_{sa}}{\rho_b V_{sb}} \text{ being the impedance ratio.}$$

The ratio of transmitted and reflected amplitudes over the incident amplitude are

$$\frac{E_a}{F_b} = \frac{2}{1+R} \text{ (transmitted) and}$$

$$\frac{F_b}{E_b} = \frac{1-R}{1+R} \text{ (reflected).}$$

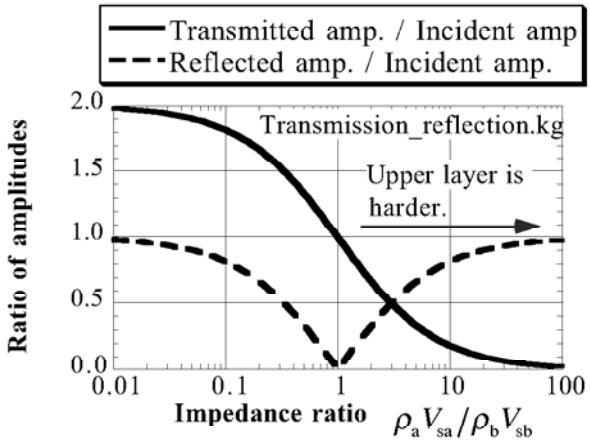

Fig. 4.23 Variation of wave amplitude at layer interface

The wave energy per one wave length is proportional to $\rho V_s E^2$ and $\rho V_s F^2$ (see Sect. 4.11). Therefore, the ratio of energy is derived in a similar way

$$\frac{\rho_a V_{sa} E_a^{\,2}}{\rho_b V_{sb} E_b^{\,2}} = \frac{4R}{(1+R)^2} \quad \text{and} \quad \frac{\rho_b V_{sb} F_b^{\,2}}{\rho_b V_{sb} E_b^{\,2}} = \left(\frac{1-R}{1+R}\right)^2.$$

These results are graphically demonstrated in Figs. 4.23 and 4.24. When the impedance ratio is 1, the material property is uniform and there is no wave reflection.

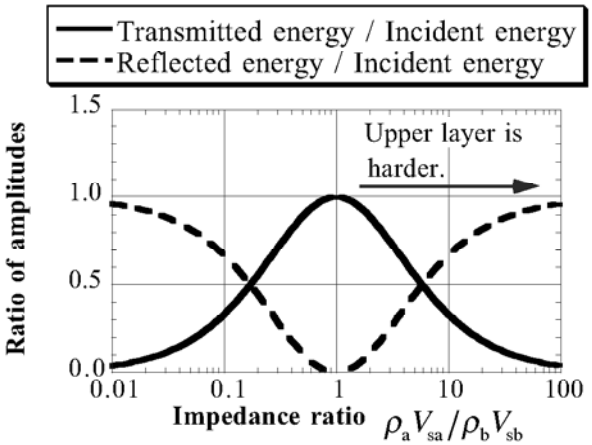

Fig. 4.24 Variation of wave energy at layer interface

4.11 Calculation of Seismic Wave Energy

Discussion here is made of S-wave propagation in the vertical direction. By assuming the displacement to be a cosine function of time, for example, displacement, velocity, and shear strain are derived

$$u = E\cos\left\{\omega\left(t+\frac{z}{V_s}\right)\right\},\quad \frac{\partial u}{\partial t} = -\omega E\sin\left\{\omega\left(t+\frac{z}{V_s}\right)\right\},\quad \frac{\partial u}{\partial z} = -\frac{\omega E}{V_s}\sin\left\{\omega\left(t+\frac{z}{V_s}\right)\right\}.$$

The wave energy per unit volume consists of kinetic and strain components

$$\frac{\rho}{2}\left(\frac{\partial u}{\partial t}\right)^2+\frac{G}{2}\left(\frac{\partial u}{\partial z}\right)^2=\frac{\omega^2E^2}{2}\left[\rho\sin^2\left\{\omega\left(t+\frac{z}{V_s}\right)\right\}+\frac{G}{V_s^2}\sin^2\left\{\omega\left(t+\frac{z}{V_s}\right)\right\}\right]$$
$$=\rho\omega^2E^2\sin^2\left\{\omega\left(t+\frac{z}{V_s}\right)\right\}=\frac{\rho\omega^2E^2}{2}\left[1-\cos\left\{2\omega\left(t+\frac{z}{V_s}\right)\right\}\right],$$

in which ρ stands for the mass density of soil. The wave energy in one wave length is derived by integrating this over the wave length ($=2\pi V_s/\omega$);

$$\text{Energy per wave length}=\frac{\rho\omega^2E^2}{2}\times\frac{2\pi V_s}{\omega}=\omega\pi\left(\rho V_sE^2\right).$$

Thus, the energy per wave length is proportional to the impedance × amplitude^2. Consequently, the energy conservation requires that the wave amplitude should increase as V_s in the medium decreases (Fig. 4.25). The amplitude is inversely proportional to the square root of wave impedance. As the wave approaches the ground surface, V_s normally decreases and the amplitude increases (Sect. 3.1). Similar to amplification of sea waves near the shore, this is one of the mechanisms of earthquake wave amplification.

The wave energy that passes through any "z" section in one period is same as above.

$$\text{Energy per one period} = (\text{Energy per volume})\times\frac{dZ}{dt}\times\text{period}=\frac{\rho\omega^2E^2}{2}\times\frac{2\pi V_s}{\omega}=\omega\pi\left(\rho V_sE^2\right)$$

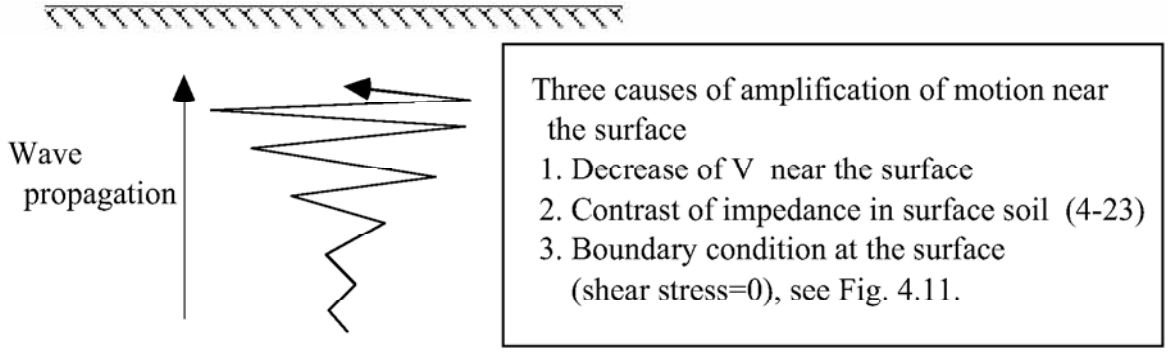

Fig. 4.25 Increase of wave amplitude with decreasing wave propagation velocity

Figure 4.21 illustrated that the major energy of Rayleigh surface wave travels in a shallow depth. Since Rayleigh wave is the major component of ground vibration caused by traffics and such construction works as pile driving, it seems adequate to install a wave insulator near the ground surface in order to mitigate this environmental noise problem.

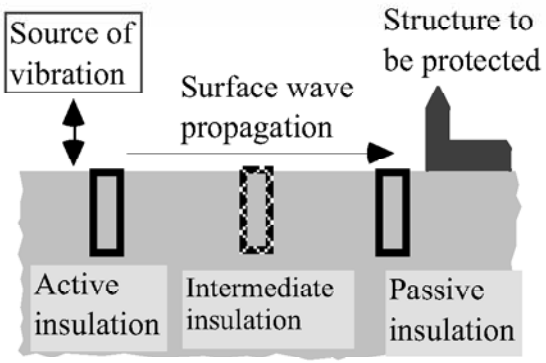

Fig. 4.26 Types of insulation against environmental ground vibration

As shown in Fig. 4.26, there are three types of mitigation. The active insulation is installed near the source of ground vibration and the cost is most probably borne by the operator or the owner of the source. On the other hand, the passive insulation is installed near the structure to be protected: paid either by the source side or by the affected party. Moreover, installation of insulation in the middle is possible. However, the land is not necessarily owned by either the source or the affected sides, and the installation is more difficult than the other two locations.

Section 4.10 discussed the energy reflection and transmission at an interface between hard and soft materials. It was shown in Fig. 4.24 that most wave energy is reflected backwards at an interface if the rigidity difference is significant. Therefore, two kinds of insulation are possible; being very rigid or very soft as compared with soil. The former is an embedded concrete wall, for example, and the latter is an open trench and embedding of other soft materials. For economical reasons, the latter appears to be more practical.

Haupt (1981) carried out model tests on an embedded rigid wall. Takemiya (2004) constructed a rigid honeycomb structure under road pavement in order to mitigate car-induced vibration.

Hayakawa et al. (1992) reduced the train-induced vibration by installing a mat under rails. The use of soft EPS can reduce the magnitude of vibration as well (Hayakawa et al. 1991). The use of gas cushion as a soft insulation was studied by De Cock and Legrand (1990) together with Massarsch (1991, 2004).

A design diagram was prepared by Woods (1968) for cut-off of surface wave propagation by a trench. The effects of a trench depend on the size of a trench and the wave length (frequency) of the concerned Rayleigh wave. The same diagram is valid for gas cushion because the same principle of cut-off is therein employed.

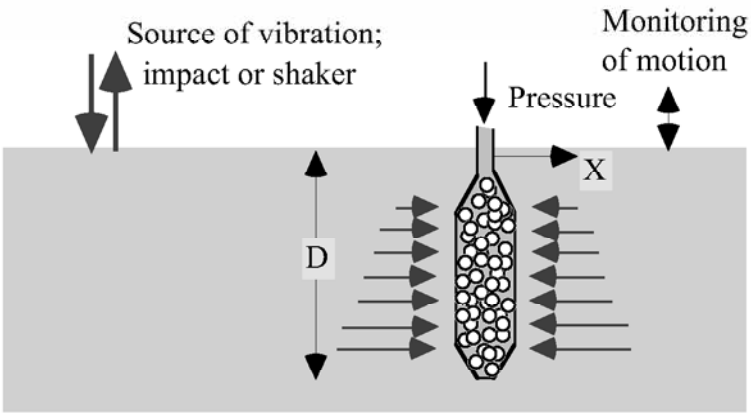

Fig. 4.27 Generation of surface wave for study of mitigation of ground vibration

The author´s group attempted to construct a similar diagram based on field tests. Ground vibration was caused either by a shaker or impact by hammer. The idea behind that study was as what follows:

- An open trench is good for mitigation of vibration, but requires a retaining structure to maintain stability. This additional structure may reduce the mitigative effects.
- Cushion, which is called air bag by the author, with internal pressure is better in this sense.

– The stability of an embedded air bag should be further improved by placing light EPS beads in a bag so that lateral resistance against earth pressure may be improved.

Figure 4.27 shows the geometry of test conditions. An air bag with EPS beads was embedded (Sannomiya et al. 1993) in order to demonstrate a relationship between wave length, horizontal distance between the point of measurement and the air bag (X), and the depth of the air bag (D). The wave length was determined by measuring the wave propagation velocity (V_r) and the shaking frequency (f);

$$\text{Wave length} = V_r / f.$$

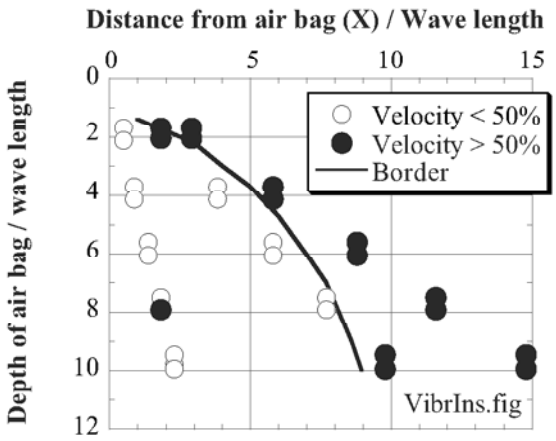

Fig. 4.28 Mitigative effects of embedded cushion under surface wave propagation (impact shaking)

The interpretation of the measured records considered that the air bag was effective when the intensity of vertical velocity was reduced to be less than 50%. Consequently, Fig. 4.28 was obtained. It is advised that the depth of an air bag is determined by referring to the curve in this figure. As the point of concern becomes further from the air bag (passive mitigation), a deeper air bag excavation is necessary.

List of References in Chapter 4

Båth, M. (1968) Mathematical Aspects of Seismology, Chap. 12, Elsevier, New York.

Bolt, B.A. (1993) Earthquakes and Geological Discovery, Scientific American Library, ISBN 0-7167-5040-6, p. 39.

De Cock, F. and Legrand, C. (1990) Ground vibration isolation using gas cushions, Proc. Int. Conf. Geotextiles, Geomembranes, and Related Products, pp. 807–812.

Haupt, W.A. (1981) Model tests on screening of surface waves, Proc. 10th Int. Conf. Soil Mech. Found. Eng., Stockholm, Vol. 3, pp. 215–222.

Hayakawa, K., Takeshita, S. and Matsui, T. (1991) Reduction effect of EPS blocks on ground vibration caused by road Traffic and its evaluation, Soils Found., Vol. 31, No. 2, pp. 226–234 (in Japanese).

Hayakawa, K., Takeshita, S. and Matsui, T. (1992) Ground vibration reduction due to vibration proof mats in railroad and its evaluation, Soils Found., Vol. 32, No. 1, pp. 249–259.

Massarsch, K.R. (1991) Ground vibration isolation using gas cushions, Proc. 2nd Int. Conf. Recent Adv. Geotech. Earthq. Eng. and Soil Dyn., St. Louis, Vol. II, pp. 1461–1470.

Massarsch, K.R. (2004) Mitigation of traffic-induced ground vibrations, Proc. 11th Int. Conf. Soil Dyn. Earthq. Eng. and the . Conf. Earthq. Geotech. Eng., Berkeley, Vol. 1, pp. 22–31.

Sannomiya, T., Towhata, I. and Kinugawa, H. (1993) Field tests on mitigation methods of ground vibration, Proc. Annual Conv. Japan. Soc. Soil Mech. Found. Eng., Vol. 1, Kobe, pp. 1261–1262 (in Japanese).

Takemiya, H. (2004) Field vibration mitigation by honeycomb WIB for pile foundations of a high-speed train viaduct, Soil Dyn. Earthq. Eng., Vol. 24, pp. 69–87.

Woods, R.D. (1968) Screening the surface waves in soils, Proc. ASCE, Vol.94, SM4, pp.951–979.

Chapter 5

Earthquake Effects

Ruin of Sacsayhuaman fortress in Cuzco, Peru. Craftsmen of Inca Empire spent one third of their working time for God, another one third on duty for the emperor, and the remaining one third for themselves. With a long working time available, the stones in the photograph were cut into very complicated shapes so that they would make perfect contact with one another. This good quality of construction made structures survive for many years without distortion.

5.1 Intensity of Earthquake Motion

Traditionally, the intensity of earthquake motion was evaluated by human senses as well as damage extents. Examples of this kind of scale are JMA scale, Mercalli intensity scale, and the MSK scale in Fig. 5.1. Since the development of earthquake monitoring instruments in more recent times, the intensity of earthquake motion started to be expressed by the maximum acceleration, the maximum velocity, the maximum displacement, a response spectrum, etc. Although the maximum acceleration is the most popular and the maximum velocity is the second, there is no single parameter that can fully take into account the nature of complicated earthquake motion.

Whichever of the above-mentioned parameters may be concerned, the intensity of motion is affected by the following issues

1. The distance from the source of motion
2. The size of rupture zone (fault)
3. The released strain energy in rock
4. Type of geology between the source and the concerned site
5. Local topography (地形) and soil conditions (locality) among others

Note that the significance and the manner of effects of these issues are variable, depending upon the choice of measures: acceleration, velocity, displacement, or others. Moreover, it has been practiced to pay attention to the extent of damage that varies with

1. The earthquake resistant design of facilities
2. Its maintenance
3. Earthquake response of facilities (intensity of motion)
4. Importance of facilities (social impact) among others

The cause and mechanism of damage vary with the type of facilities. Hence, it is impossible to select any single parameter to describe the intensity of earthquake from the view point of observed damage. However, it has been practiced widely to use one type of intensity for convenience.

Seismic intensity is determined by taking into account

1. How strong the earthquake motion was FELT
2. Extent of structural damage
3. Extent of ground failure (cracking etc.)

Evidently, the intensity depends upon the locality.

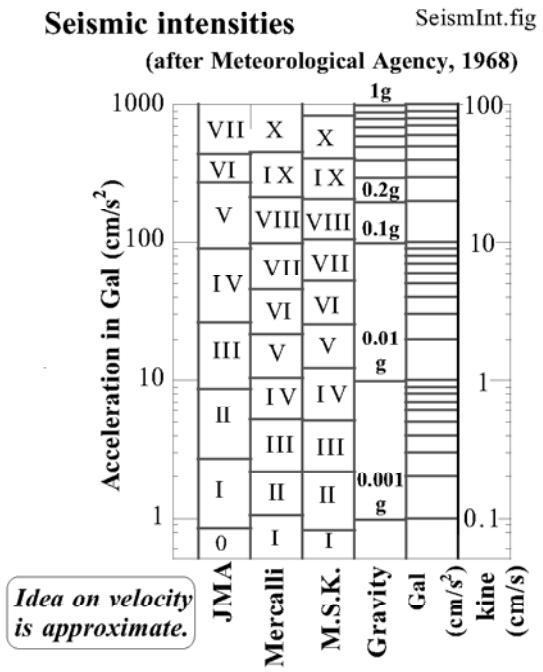

Fig. 5.1 Comparison of seismic intensity scales (Velocity value is approximate) (Meteorological Agency, 1968)

Three kinds of seismic intensity scales are compared in Fig. 5.1: JMA scale (Japanese Meteorological Agency 気象庁震度), abridged modified Mercalli intensity scale (MM scale), and the MSK scale. They are roughly related to the maximum acceleration and velocity.

Any scale is affected by the local topography and geological conditions at earthquake observation stations. The determined intensity may not be related with the regional extent of damage.

Recently a new seismic intensity scale has been developed in European countries. Being called EMS

scale (European Macroseismic Scale), it has 12 divisions, each of which is defined based on human response and extent of damage. Thus, the basic principle is identical with those of classic scales. This scale is briefly summarized in what follows; for details, refer to the original definition (http://geology.about.com/library/bl/blems.htm).

Table 5.1 Definition of European macroseismic scale

Scale	Rank	Brief description
1	Not felt	
2	Scarcely felt	Felt only by people at rest in house
3	Weak	Felt by a few people
4	Largely observed	Felt indoors by many people but not much felt outdoors. Swinging of objects is detected
5	Strong	Buildings shake; glasses clatter, and top heavy objects turn down
6	Slightly damaging	People are frightened and slight damage to many ordinary buildings such as fine cracks
7	Damaging	Most people are frightened, furniture move, and objects fall down. Moderate damage to ordinary buildings such as small cracks
8	Heavily damaging	Overturning of furniture. Buildings suffer large cracks and possibly collapse
9	Destructive	Partial collapse in many ordinary buildings and complete collapse in a few of them
10	Very destructive	Many ordinary buildings collapse
11	Devastating	Most ordinary buildings collapse
12	Completely devastating	Almost all structures, both above and below ground, are heavily damaged or destroyed

5.2 Revised Earthquake Intensity

The JMA scale in Sect. 5.1 was revised in 1996 from human observation of earthquake effects (shaking and damage extent) to instrumental observation. The new JMA scale 新しい気象庁震度 is determined by a specially developed equipment 震度計. This scale is, however, still correlated literally with observed phenomena as what follows.

Measured scale	Human effects	Effects on lifelines	Effects on ground and slope
0	Nothing felt		
1	Felt by some people, if staying indoor		
2	Felt by many indoor people. Some sleepers are awaken		
3	Felt by most indoor people; possible to be frightened		
4	Frightened. Some may try to escape		
Lower 5	Many try to escape, but not easy 身の安全を図ろうとしても 一部の人は行動に支障	Gas supply is cut by a home safety system. Water supply and electricity may be lost	Possible cracking in soft soil. Stone fall and small landslide are possible in mountains
Higher 5	Substantially frightened. Cannot move easily 非常な恐怖、行動に支障	Minor gas pipes and major water pipes can be broken	ditto 上に同じ
Lower 6	Cannot stand upright 立っていることが困難	ditto	Cracks and landslides occur 亀裂と山崩れ
Higher 6	Can only crawl 這うのがやっと	Major gas pipelines and water treatment facilities are damaged	ditto
7	Cannot control one's body	Overall loss of electricity, gas, and water	Large cracks and landslides occur

This revised seismic intensity is determined by special instruments. Its details are described in Sect. 5.3. Thus, the human judgment of the scale was terminated.

5.3 Instrumental Determination of Seismic Intensity

The JMA (Japanese Meteorological Agency) scale of seismic intensity is today determined by electronic instruments that monitor on a real-time basis the seismic motion. A special attention was paid by JMA to maintain the consistency of the intensity between the former human and new instrumented procedures. Moreover, the quick determination of the seismic intensity immediately after the shaking is important.

The new procedure relies on a time history of acceleration, which probably best accounts for the damage extent. Figure 5.2 illustrates the schematic idea of the procedure. The three time histories in *NS*, *EW*, and *UD* directions are processed by digital filters. Figure 5.3 shows the effects of three digital filters and their combination, which remove both high- and low-frequency components from the acceleration records. The formulae of filters are;

Low-pass filter $F_1 = \sqrt{1/f}$

High-cut filter

$$F_2 = 1\Big/\sqrt{\begin{array}{c}1+0.694X^2+0.241X^4+0.0557X^6\\+0.009664X^8+0.00134X^{10}+0.000155X^{12}\end{array}}$$

Low-cut filter $F_3 = \sqrt{1-\exp\left\{-\left(f/f_o\right)^3\right\}}$,

in which f is the frequency (Hz), $X = f/f_c$, f_c = 10 (Hz), and f_o =0.5 (Hz). Hence, the total effects are given by $F_1 \times F_2 \times F_3$.

Then, three records are added in a vector manner to obtain a scalar (positive) time history, Accel*(t).

The representative amplitude of Accel* is designated by a_o and is determined by the method in Fig. 5.4. The time in which Accel* is greater than the threshold value, a, is shown by ——— in Fig. 5.4 and its total value is plotted against "a." The total time decreases as "a" increases, and a_o is the particular a value for which the total time is $\tau_o = 0.3$ s.

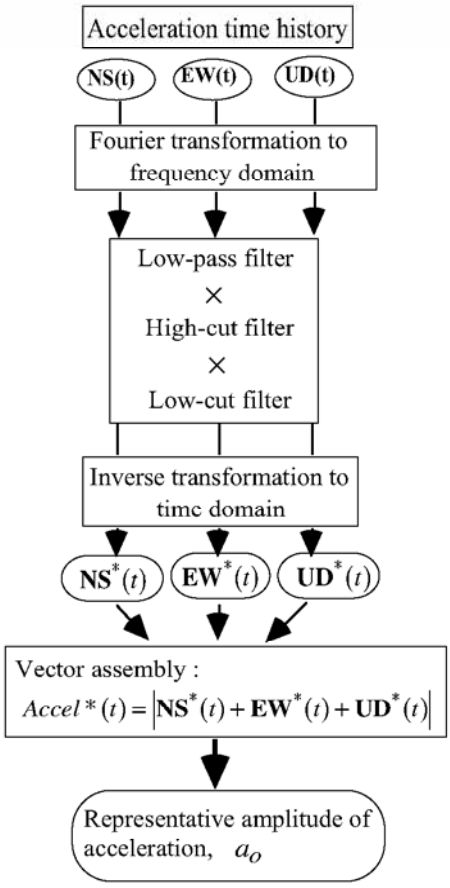

Fig. 5.2 Determination of instrumental seismic intensity

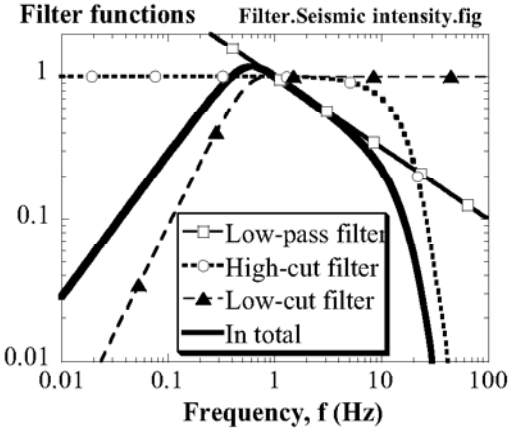

Fig. 5.3 Effects of digital filters

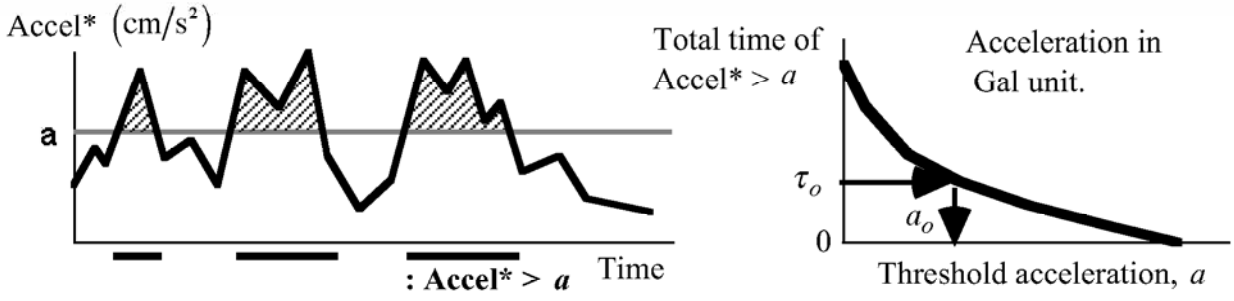

Fig. 5.4 Determination of representative amplitude of irregular time history

This a_o (cm/s^2) is finally substituted in

$$I = 2\log_{10}(a_o) + K,$$

where I is the instrumental seismic intensity and K=0.94.

Although this instrumental seismic intensity was designed to be equivalent with the traditional one (Sect. 5.2), it is felt that the new one is greater than the conventional one by roughly 0.5; real damage is not so severe as suggested by the instrumental seismic intensity.

5.4 Earthquake Magnitudes

Since the seismic intensity highly depends on locality, it is not suitable to describe the size of an earthquake by this intensity. The size of earthquake is more appropriately evaluated by "earthquake magnitude M," which has several versions. One group of magnitudes depends on the intensity of earthquake shaking, in terms of energy or amplitude, as generated by the fault rupture zone, while the other group on the extent and size of distortion in the earth crust of the rupture zone (Utsu, 1999). Note that a detailed discussion on magnitudes is extremely complicated and difficult.

1. Local magnitude (Richter scale), M_L (Richter, 1935)

This is the first idea of earthquake magnitude defined by

$$M_L = \log_{10}\{a(\Delta)/a_0(\Delta)\},$$

in which Δ is the epicentral distance (km), $a(\Delta)$ is the amplitude of record on paper obtained by a then available Wood-Anderson seismograph, and $a_0(\Delta)$ is the amplitude of a standard earthquake (defined to have M_L=1.0) at the same site. The standard earthquake is the one that gives a = 1 mm at Δ = 100 km. Thus, the local magnitude is a ratio of a given and a standard earthquake intensity. By using a Californian empirical formula valid for Δ < 600 km : $\log_{10}a_0$ = 6.37-3$\log_{10}\Delta$, together with the nature of the Wood-Anderson instrument a=2800×A in which "A" is the maximum ground displacement in mm unit,

$$M_L = \log_{10}A + 3\log_{10}\Delta - 2.92.$$

This makes it possible to determine the Richter-scale magnitude in the Californian locality without a specified instrument. Empirically, $M_L > 7$ is very rare (Utsu, 1999). In the recent times, the *W-A* instrument is not available, and media reports M_L as converted from other kinds of magnitude.

2. JMA (Japanese Meteorological Agency) magnitude, M_{JMA}

This magnitude is calculated by

$$M_{JMA} = \log_{10}A + 1.73\log_{10}\Delta - 3.83$$

and is intended to be equivalent with the Richter scale. For the calculation of this magnitude, the single amplitude of displacement as recorded by an instrument is divided by the amplification of the instrument, and the amplitude of the ground displacement, A (mm unit), is obtained.

3. Kawasumi magnitude M_k (Kawasumi, 1951)

Since the geological time scale is very long, the local seismic activity can be studied only by using historical earthquake information. Because of lack of measured intensity of seismic motion, Kawasumi (河角 1951) used the assessed JMA scale of seismic intensity (Sect. 5.2), which was determined by interpreting historical documents on damage. He defined the first version of his seismic magnitude, M_k, as the JMA scale at the epicentral distance of 100 km. He then found an empirical correlation between his magnitude and Richter magnitude (M_L) as

$$M_L = 4.85 + 0.5\,M_k\ .$$

In the recent times, $4.85 + 0.5\,M_k$ is called the (revised) Kawasumi magnitude and is widely referred to.

4. Surface wave magnitude M_S (Richter, 1945a)

This magnitude suits a shallow earthquake, which is recorded at a far distance. The measured seismic motion record is dominated by surface wave propagation of a long period (about 20 s) (Sect. 4.7). This magnitude can hardly exceed the value of 8. Hence, it is not suitable for a gigantic earthquake.

5. Body wave magnitude, m_b (Richter, 1945b and 1945c)

This magnitude suits a deep earthquake. It is determined by using P and S waves (body waves, Sect. 4.2). These waves have predominant periods of about 1 s.

6. Earthquake energy E (erg = 10^{-7} J)

$$\log_{10}E = 1.5M_{\mathrm{JMA}} + 11.8 \qquad \text{empirically.}$$

When M_{JMA}=6.5, E=3.5×10^{21} and when M_{JMA}=7.5, E=1.1×10^{23}. When the magnitude increases by 1, the energy increases 32 times. Utsu (1999) summarized many empirical relationships between earthquake energy and earthquake magnitudes.

7. Moment magnitude, Mw

This magnitude is related with the earthquake moment, M_0. It considers the stress state in the fault before the breakage together with the fault size. The earthquake moment is defined by

$$M_0 = G_{\mathrm{earth}} \times (\text{Fault displacement } D) \times (\text{Fault area}) \quad \text{(unit : dyne and cm)}$$

in which G_{earth} stands for the shear modulus of earth crust. Accordingly,

$$M_{\mathrm{w}} = (\log_{10} M_0 - 9.1)/1.5 \ .$$

The moment magnitude is used to express the magnitude of gigantic earthquakes.

5.5 Time History of Ground Motion

It is a frequent practice for earthquake engineers to talk about the time history of acceleration and its maximum value. This comes from the principle of d´Alembert in mechanics, which states that a base acceleration is equivalent with an inertia force (Fig. 5.5). There are, however, different viewpoints in interpreting the significance of given seismic records.

In 1995, a velocity time history was recorded at University of Kobe on a rock outcrop (CEORKA: The Committee of Earthquake Observation and Research in the Kansai Area). A time-derivative of this record gave an acceleration history, while it was integrated with time to be a displacement record. Figure 5.6 compares the acceleration and displacement thus obtained. The maximum acceleration (A_{max}) was 270.3 Gal, Gal=cm/s^2. It seems clear that the acceleration time history has a significantly shorter period or a higher frequency than the displacement record does. The reason for this is found in an example of a harmonic motion.

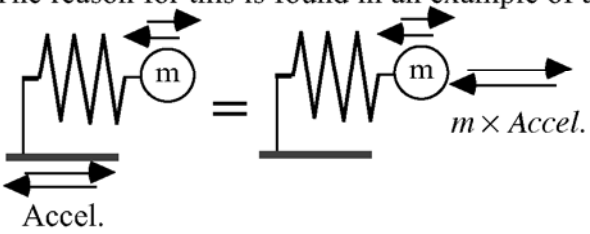

Fig. 5.5 d´Alembert's principle

When a velocity record, v, is given by

$$v = v_0 \sin \omega t$$

the displacement (d) and the acceleration (a) records are expressed as

$$d = \int_0^t v_0 \sin \omega\tau \, d\tau = \frac{v_0}{\omega}(1 - \cos \omega t)$$

$$a = \mathrm{d}v/\mathrm{d}t = \omega v_0 \cos \omega t \ .$$

Note that the amplitude of the acceleration record is ω^2 times greater than that of the displacement. This ratio (ω^2) increases for a greater value of ω, i.e. a higher frequency. Therefore, an acceleration record intensifies high frequency components, while low frequency components are predominant in a displacement record.

This feature is clearly seen in Fig. 5.6 where the original velocity record was differentiated and integrated with time to obtain acceleration and displacement, respectively. The predominant period of acceleration is much shorter than that of displacement.

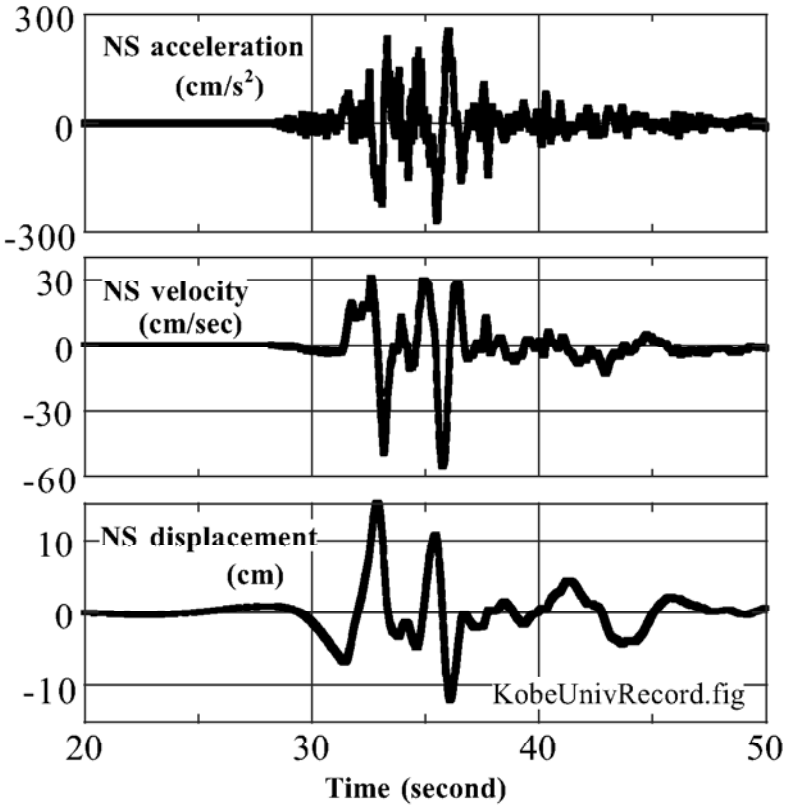

Fig. 5.6 Velocity time history of Kobe earthquake in Kobe University and its differentiation (acceleration) and integration (displacement) (CEORKA)

5.6 Effects of Local Soil Conditions on Maximum Acceleration

The intensity of earthquake motion depends on the following issues:

- Type of record; displacement, velocity, or acceleration
- Magnitude of earthquake (released energy)
- Direction and distance from the source fault
- Topography; plain, mountain, top and bottom of cliff, valley, etc.
- Local geology

With regards to the local geology, an alluvial deposit (沖積地盤) together with an artificial ground (人工島など) is generally associated with a stronger maximum acceleration. Figure 5.7 illustrates the maximum horizontal acceleration values recorded in the San Francisco Bay area, which was shaken by the 1989 Loma Prieta earthquake. The epicenter is located near the bottom of the figure, and the Bay area in the upper half of the figure is of more or less the same epicentral distance. With other things same, the area of softer subsoil along the bay coast had stronger acceleration than hilly and mountainous areas. It seems, therefore, that a softer deposit amplifies the earthquake motion.

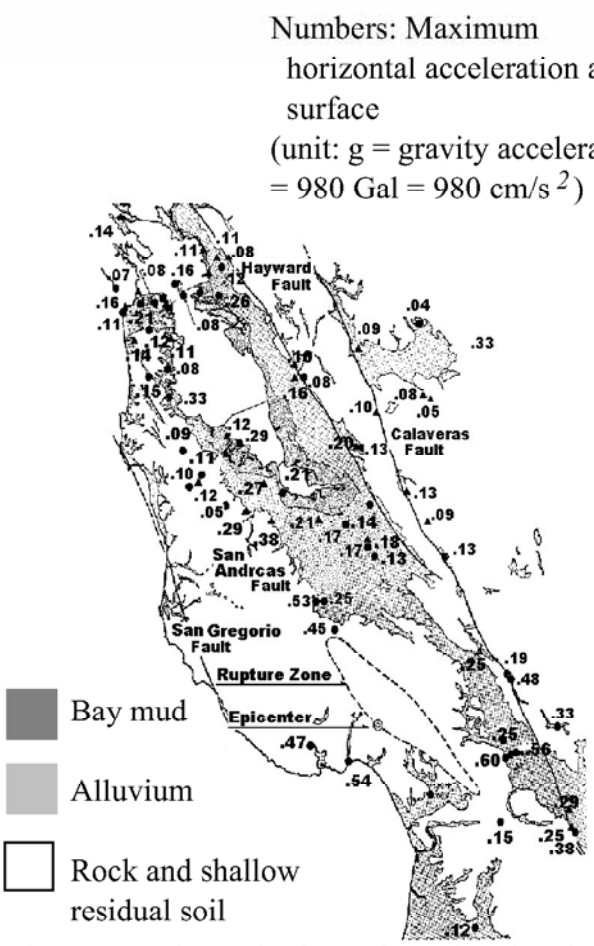

Fig. 5.7 Maximum horizontal acceleration during 1989 Loma Prieta earthquake (original figure by Seed et al., 1991)

The recent experience in Kobe in 1995 is not in line with San Francisco probably because the damaged area was above or very close to the causative fault, and the epicentral distance was more important than the local soil condition. Another reason is that the three-dimensional structure of base rock made a complicated propagation and reflection of seismic waves that could govern the intensity of surface motion.

There is a case in which the surface soft soil deamplifies (makes weak) the earthquake motion. This occurs when the energy loss during the propagation of the earthquake wave towards the surface is very significant and the motion loses its amplitude; for example, the surface soil is a soft mud or a liquefied sand (Sect. 17.12). Another example is a propagation of very strong motion that produces a large amplitude of stress and strain; see Sect. 9.1 etc. for ideas on damping ratio.

5.7 Some Famous Earthquake Motion Records

See Figs. 5.8–5.11 for several famous acceleration records.

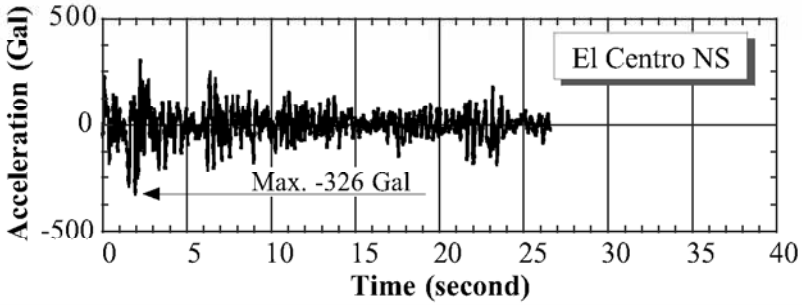

Fig. 5.8 *El Centro* motion is the first-ever-recorded strong earthquake motion. This record has been widely used in earthquake-resistant design of structures

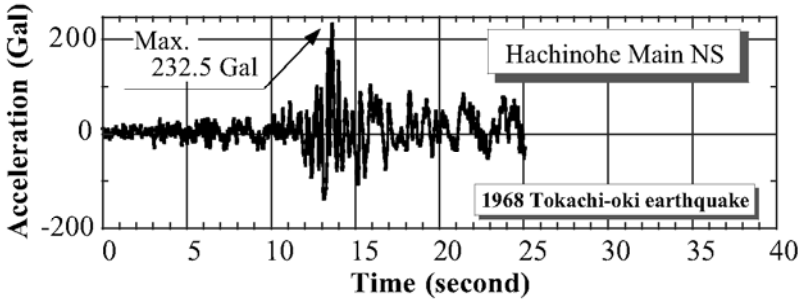

Fig. 5.9 *Hachinohe* record during the 1968 Tokachi-oki earthquake is famous for its elongated period. This is an important input motion for analysis on structures that have a long natural period

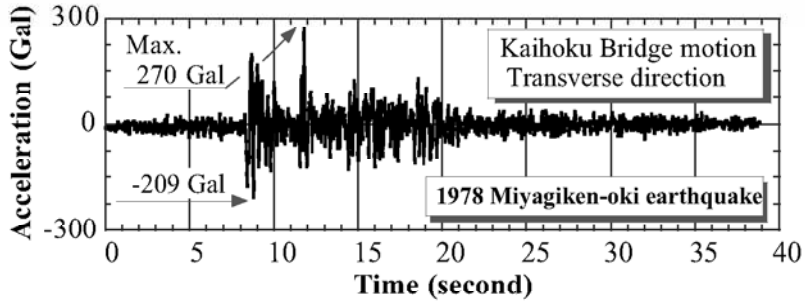

Fig. 5.10 *Kaihoku* (開北) motion during the 1978 Miyagiken-oki (宮城県沖) earthquake. This record has been considered to be a rock outcrop and has, therefore, been used as a typical input motion into surface deposits. Actually, the observation station for this record is close to a bridge pier and is situated on soil. For significance of outcrop motion, see Sect. 6.8

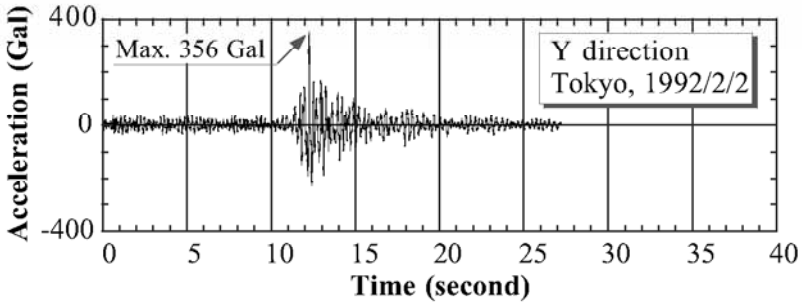

Fig. 5.11 This record was obtained at a top of a *small hill in Tokyo* during a minor earthquake. No damage was caused by this. The maximum acceleration is, however, as large as 356 Gal (cm/s^2) which is compatible with the maximum acceleration in other three records in this section. Thus, the intensity of maximum acceleration is not a fully-reliable damage parameter

The 1985 Mexican earthquake is famous for heavy damages in buildings in the Mexico City. Although this city was located at 390 km from the fault area, the capital city suffered an unexpectedly significant damage. Figure 5.12 compares the acceleration records that were obtained in the Mexico City basin (Central de Abastos) and at the Pacific coast near the fault (Zacatula and Caleta de Campos). It is evident that the motion in the Mexico City had a longer period (approximately 3 s.) and an elongated duration time of shaking. Figure 5.13 shows that some sites in the Mexico City area were shaken by an extraordinarily strong magnitude of acceleration.

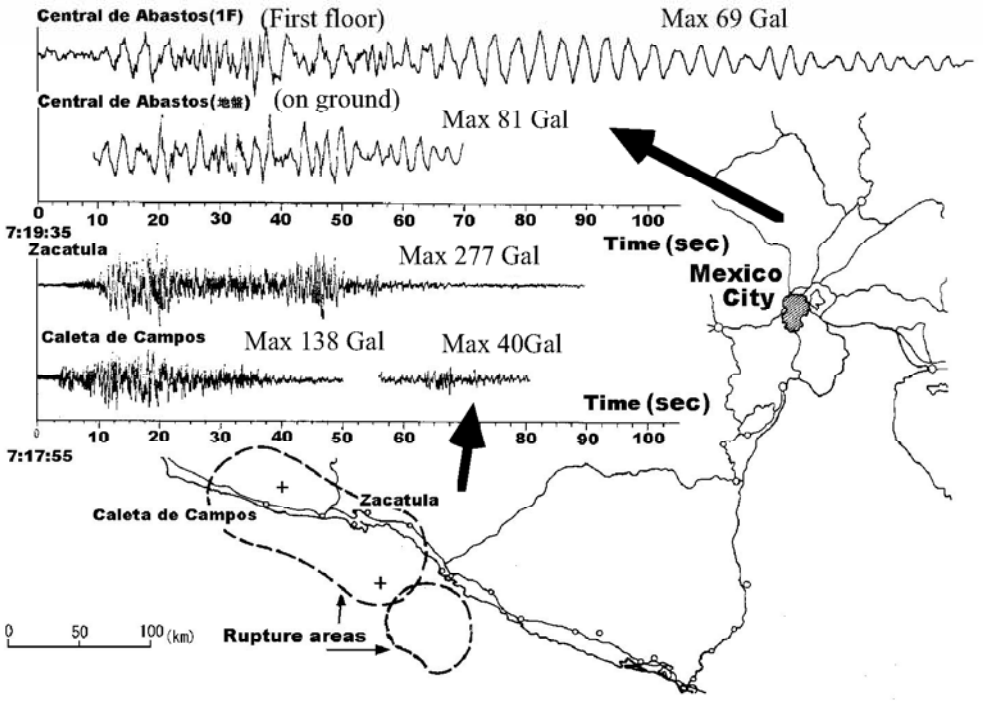

Fig. 5.12 Ground motion records near the fault and the Mexico city basin (after Tamura et al., 1987)

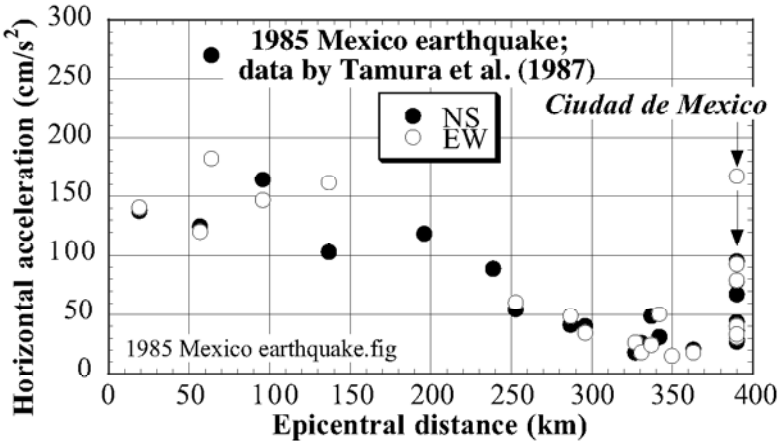

Fig. 5.13 Strong motion in Mexico City at the longest distance

It is believed today that the locally strong ground motion was caused by the soft deposit of soil in the city. The Mexico City basin used to be a big lake, which was buried naturally and artificially after a long period of time. Being famous for big consolidation settlement, the Mexico City clay has a natural water content (Sect. 1.2) of 300–600% while its thickness is variable (Mendoza and Romo, 1998). In this respect, the following points are important.

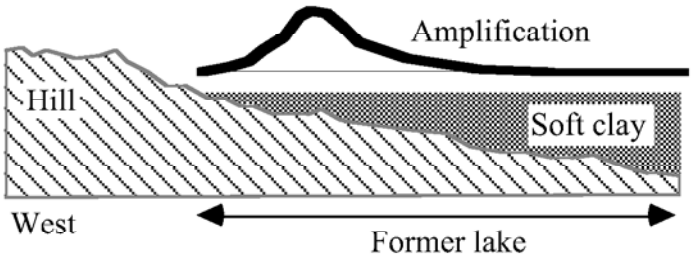

Fig. 5.14 Schematic diagram on localized strong earthquake response in Mexico City

- The thickness of soft soil in Mexico City basin increases from zero at the western edge to tens of meters in the middle of the basin.
- The natural period of ground depends not only on the stiffness of soil but on the thickness of soft soil.
- The earthquake motion of the same period as the natural period of ground is amplified (made stronger).
- At the critical place where the natural period and the predominant period in the earthquake motion matched, a significant amplification occurred, leading to building damage, see Fig. 5.14.
- Earthquake energy was trapped by the soft deposit, leading to long duration of free shaking.

After the experience of Kobe earthquake in which location of damaged houses was localized (see Sect.

5.14), a different idea was proposed. Figure 5.15 illustrates a soft alluvial deposit staying on a concave interface with base rock. Since the wave propagation velocity is higher in the rock than in the upper soil, the direction of wave propagation is refracted at the interface (Snell´s law) and the earthquake energy is focused on some point. Being called the edge effect, this situation induces damage concentration on a narrow area along the foot of a mountain.

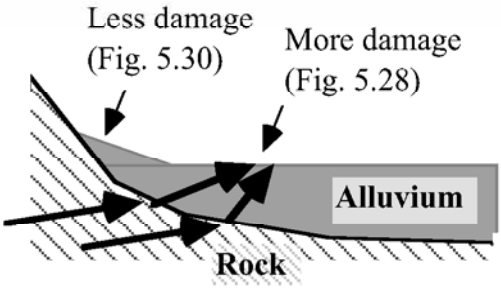

Fig. 5.15 Focusing of seismic energy due to concave underground structure

5.9 Power of Acceleration Time History

The destructiveness of an earthquake motion is most reasonably evaluated by its effects on residual deformation or energy dissipation within a given structure. Since real structures are substantially variable in the sense of size, shape, and rigidity, it is good to replace them by a single-degree-of-freedom model, see Fig. 5.16. Housner's spectrum intensity (SI in Sect. 23.2; Housner, 1961) stands for the magnitude of relative velocity between the base and the top mass of this model and designates the extent of distortion and damage.

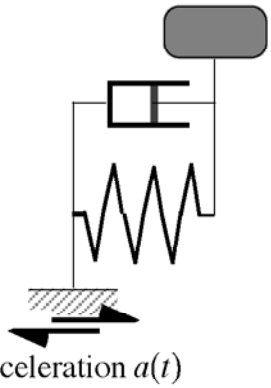

Fig. 5.16 Single-degree-of-freedom model

Arias (1970) stated that the energy dissipation, I, per unit weight of a single-degree-of-freedom model is given by

$$I = \frac{f(\mu)}{g} \int_{\text{beginning}}^{\text{end}} \text{acceleration}^2 \, \mathrm{d}t = \frac{\arccos \mu}{g\sqrt{1-\mu^2}} \int_{\text{beginning}}^{\text{end}} \text{acceleration}^2 \, \mathrm{d}t, \tag{5.1}$$

where μ is the critical damping ratio of the model, and g is the gravity acceleration, while the integration is made from the beginning till the end of a given acceleration time history. Being called Arias intensity, this I has a unit of velocity. For practice, the value of $f(\mu)$ is not much affected by the choice of the critical damping ratio (Fig. 5.17) and, hence, the type of a concerned structure. Since Arias did not present the derivation of (5.1), a detailed discussion on it is impossible. It is, however, subject to a question why an undamped model (μ=0) still makes $f(\mu) > 0$ and energy is dissipated in the model.

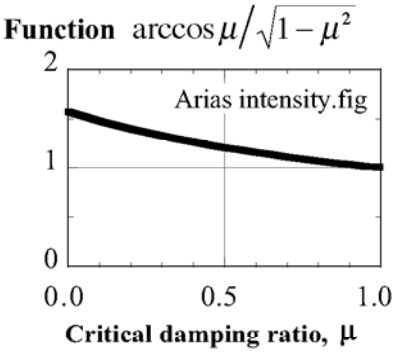

Fig. 5.17 Effects of critical damping ratio on Arias intensity

A simplified version of (5.1) is called the power of acceleration time history

$$\text{Power} = \int_{\text{beginning}}^{\text{end}} \text{acceleration}^2 \, \mathrm{d}t. \tag{5.2}$$

"Power" is more closely related with the destructiveness of an earthquake motion time history than the maximum acceleration because the duration time and probably the number of loading cycles are somehow taken into account. On the contrary, the power does not pay attention to the fact that soil (an elastoplastic material) develops the largest deformation during the first cycle if the amplitude of loading is uniform during a sequence of loading (Fig. 5.18). Thus, the order of loading is out of scope of the power.

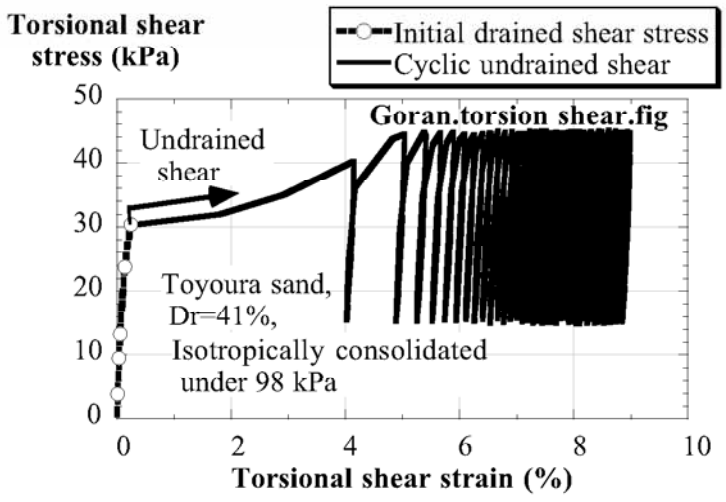

Fig. 5.18 Undrained cyclic loading on Toyoura sand with initial shear stress (Arangelovski and Towhata, 2004)

5.10 Distance From Source of Earthquake

It is well known that the intensity of shaking decreases as the distance increases from the seismic fault or the rupture of the earth where the earthquake shaking is generated. To quantitatively take into account the effects of distance into engineering practice, it is important to define the distance quantitatively. Figure 5.19 illustrates different ideas of distance parameters.

Definitions of terms:

Epicenter 震央: place at the earth's surface lying above the hypocenter.
Hypocenter 震源: part of fault where rupture starts.

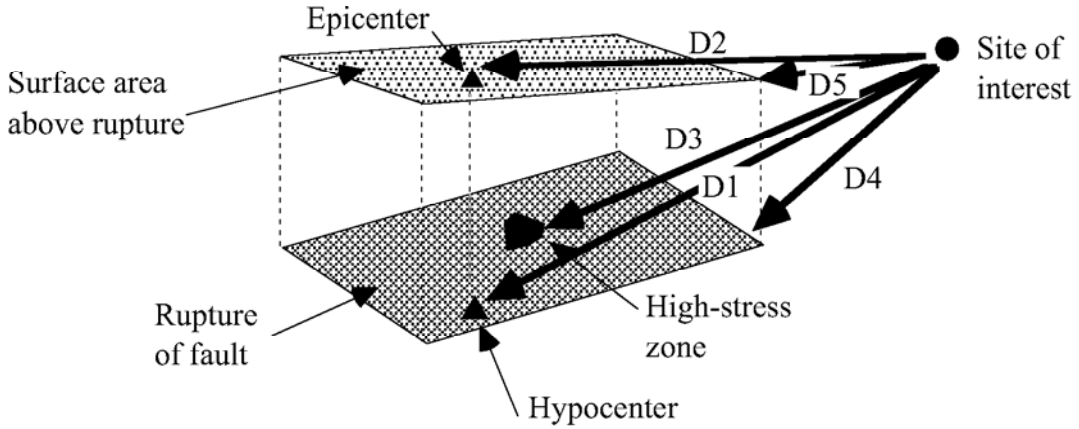

D1: hypocentral distance.
D2: epicentral distance.
D3: closest distance to high-stress zone (possibly most seriously ruptured part of fault).
D4: closest distance to edge of fault rupture.
D5: closest distance to surface projection of rupture.

Fig. 5.19 Illustration of parameters defining distance from an earthquake source to the place of interest (station) at the earth surface (original figure was drawn by Joyner and Boore, 1996)

Among five indices of distance, the epicentral distance (D2) has been used in many situations. Recently, however, the distance to the edge of a fault (D4) has been considered to be important; this is particularly the case at a short distance where the epicentral distance is large but the distance to the fault is short, leading to severe intensity of shaking.

5.11 Estimation of Intensity of Earthquake Motion

It is an interesting research to estimate the nature of future earthquakes by using information on potentially active seismic faults. One of the most rigorous approach to this goal is a use of fault rupture model combined with calculation of seismic wave propagation from the fault to the site of concern. This approach is, however, not able to assess acceleration for which higher frequency components are important for practice (Sect. 5.5).

Another approach is an empirical correlation between such a feature of earthquake motion as maximum velocity or acceleration and distance from the epicenter (or fault), while taking into account the seismic magnitude (Sect. 5.4). This issue stands for the decay of earthquake motion intensity and otherwise called attenuation curve (距離減衰). An early example was proposed by Kanai and Suzuki (1968) between maximum velocity and hypocentral distance (Fig. 5.19). Note that the concerned ground velocity was the one in the base rock underlying surface soil. Hence, the amplification in the surface soft soil was out of scope.

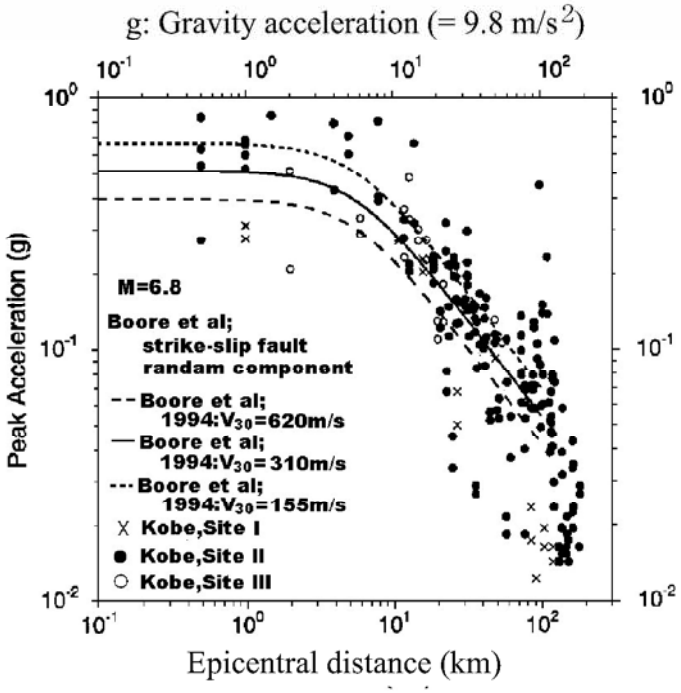

Fig. 5.20 Empirical correlation between observed maximum horizontal acceleration and distance from the surface area lying above the fault; V_{30} means the average V_S in the surface 30 m of deposit (Joyner and Boore, 1996)

Figure 5.20 is another example correlation between epicentral distance and peak acceleration. It is important that the observed earthquake motion at the shortest distance from the fault of less than 3 km is included. Such a data became available since 1990s when many earthquake observation stations were deployed. Note that the acceleration near the fault is not affected by distance any more. Further, it should be borne in mind that the intensity of shaking and this type of correlation vary with the local soil types; normally soft soil deposits (V_s=155 m/s in Fig. 5.20) exhibit greater intensity of shaking than harder soil deposits (V_s= 620 m/s in Fig. 5.20). Therefore, a suitable correlation should be chosen for practice. It is important that the surface acceleration is even reduced by subsurface liquefaction (Sect. 18.9).

Many empirical correlations have been proposed for response spectrum (Sect. 23.1) and maximum velocity among others; being improved today by adding recent data at short distance from faults. Since such an earthquake feature is affected by the amplification of ground motion in the surface geology, different surface soil conditions require different correlations to be used.

Because of the increasing number of earthquake observation stations, the above-mentioned correlation with the distance is being improved after every earthquake event. Therefore, it is necessary to use as recent as possible correlations for an earthquake hazard analysis.

5.12 Estimation of Duration of Earthquake Motion

Duration time of strong shaking plays an important role when the accumulated effects of shaking are of major concern. Some of the examples of this kind of phenomenon is a development of deformation of earth structure with the number of cycles or time. Another important example is liquefaction.

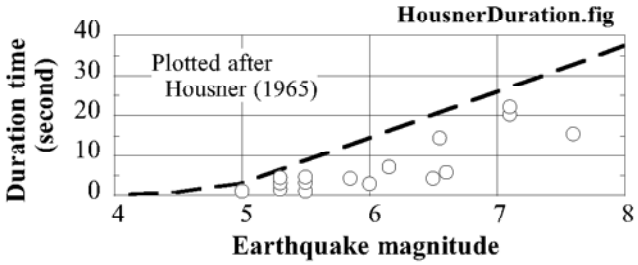

Fig. 5.21 Empirical estimation of duration time of strong motion (Housner, 1965)

Figure 5.21 by Housner (1965) exhibits the duration time of strong motion, although he did not clearly define what the strong motion stands for.

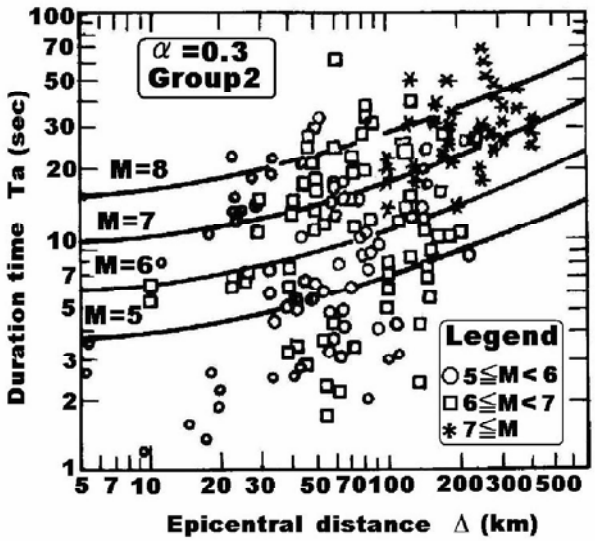

Fig. 5.22 Empirical correlation on relatively stiff ground between duration time of strong shaking and distance (Kawashima et al., 1985)

Figure 5.22 shows a correlation between duration time of strong shaking and the epicentral distance. Noteworthy is that Figure 5.22 concerns with the time period in which the amplitude of acceleration is greater than 0.3 times the maximum acceleration. Hence, no threshold acceleration level (e.g. 50 Gal) is intended. Also, the data was obtained upon relatively stiff soil.

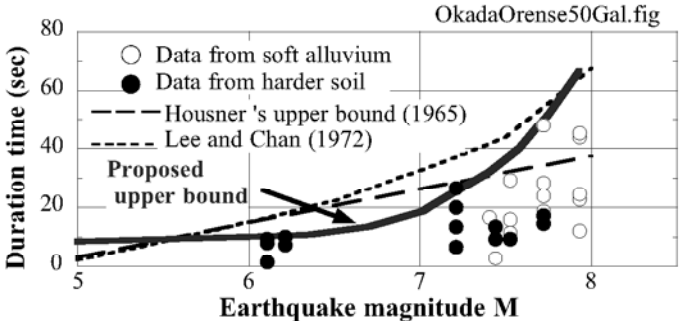

Fig. 5.23 Duration of acceleration greater than 50 Gal after maximum acceleration (Okada et al., 1999)

Okada et al. (1999) analyzed many earthquake motion records to study the duration of horizontal acceleration greater than 50 Gal after the maximum acceleration (Fig. 5.23). It is in contrast with Housner (1965) as well as Lee and Chan (1972) who were simply interested in duration of strong motion (>50 Gal in case of Lee and Chan). This study was particularly related to evaluation of liquefaction-induced ground flow. Noteworthy is the threshold acceleration of 50 Gal irrespective of the maximum acceleration. About 50 Gal was tentatively chosen because it is half of 100 Gal that is approximately the minimum acceleration needed to trigger liquefaction in loose sandy deposits. The obtained duration time depends upon the distance from the fault, which is not yet considered in the figure, as well as the magnitude in the horizontal coordinate. Hence, the upper bound of the data is used for practice.

5.13 Determination of Design Earthquake Motion

In the tradition, design earthquake was simply specified by the seismic coefficient (Sect. 7.1), which is somewhat equivalent with the maximum acceleration during one shot of shaking. That practice was sufficient in the previous times because the engineering concern lay in the possibility of collapse: factor of safety greater or less than 1.0. In the recent times, however, the seismic performance of structures is very important (Sect. 14.5), and more detailed design earthquake such as time history of acceleration has to be prepared. Note that studies on time history of design earthquakes mostly concern with the motion on rock. Thus, the effects of surface soil has to be investigated separately.

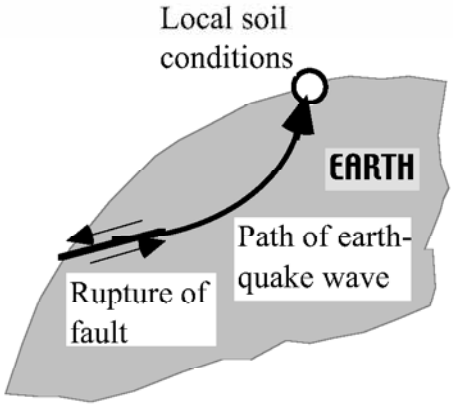

Fig. 5.24 Relationship between causative fault, intermediate path, and local soil conditions

First of all, it should be stated that different kinds of design earthquakes are employed in practice. When safety against earthquakes that occur at least once during the life span of a concerned structure (probably once every fifty years or so), the employed design earthquake is not extremely strong. It is therein desired that a structure should maintain its function and nobody is injured by such an event. It is also important to pay attention to a very rare but extremely strong earthquake. Probably such an event occurs once every 500 or 1,000 years (return period = 500–1,000 years or longer). Under such an extreme situation, damage is allowed to some extent. However, a total collapse has to be avoided. To achieve this goal, the design earthquake is very strong as well. This topic will be discussed again in Sect. 14.7.

An earthquake motion is generated by rupture of a fault. This motion propagates in the earth, reaches its surface, and causes shaking. This surface shaking changes its intensity according to such local conditions as types of surface deposits, stiffness of soils, and the thickness of the surface soils. Figure 5.24 illustrates that the characteristics of the surface earthquake motion are composed of three factors: the fault characteristics, the nature and length of the intermediate path, and the local soil conditions. Thus, it has been an attractive idea to take into account these three components and predict the time history of earthquake motion at the earth's surface. In a mathematical form,

$$R(\omega) = F(\omega) \times P(\omega) \times L(\omega), \qquad (5.3)$$

where $R(\omega)$ designates the observed earthquake response at the surface which is a function of frequency or circular frequency (ω = frequency/2π). $F(\omega)$ stands for the fault mechanism and varies with the seismic activity of the concerned fault. $P(\omega)$ designates the effects of the intermediate path and reduces the intensity of motion as the distance from the fault becomes longer. Finally, $L(\omega)$ is the effects of surface soil deposits (amplification effects). In principle, the surface earthquake motion can be predicted by taking into account three factors on the right-hand side of (5.3).

The identification of the local soil effects, $L(\omega)$, has been one of the major topics of soil dynamics. To date, this issue is understood to a substantial extent (Chaps 9 and 10). Remaining issues concern the technologies for in-situ soil investigation. The nature of $P(\omega)$ has also been understood in detail by reasonably assuming that the earth is made of isotropically elastic media. In contrast, the nature of fault, $F(\omega)$, still has many to be studied. It appears to the author that the present understanding on $F(\omega)$ is limited to a range of lower frequency. Above 1.0 or 1.5 Hz, the nature of the fault-generated earthquake motion cannot be predicted. This implies that the acceleration cannot be predicted by (5-3), while displacement can be reproduced analytically by using a fault mechanism model. The research in this

direction is still on-going for further development.

Since the practical use of (5.3) appears difficult, attempts have been made to propose alternative methods. One of them is an empirical determination of $F(\omega) \times P(\omega)$ by observing earthquake motions generated by smaller but more frequent earthquakes in the same fault area (Fig. 5.25). Since a larger earthquake is produced by a bigger fault action with a greater rupture displacement, it is predicted by assembling motions that are produced by a number of small fault mechanisms. In the present engineering, the motion proposed by a small fault action is called Green's function (for example, Kobayashi and Midorikawa, 1982; Irikura, 1983, 1986). It is necessary not only to add the motion made by a small fault but also to consider the effects of greater fault displacement and the consequent elongated duration and the elongated period.

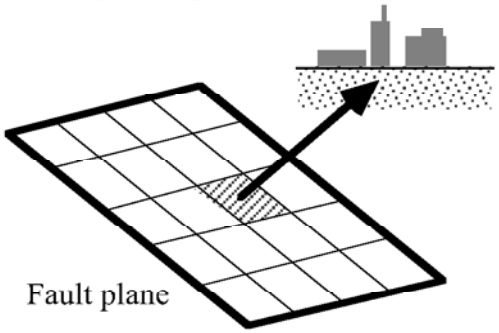

Fig. 5.25 Individual effect of small fault rupture on earthquake motion

Another approach is the use of empirical relationships between the epicentral distance and the maximum acceleration, velocity, response spectra, and others (see Sects. 5.11 and 5.12). In this method, the initial time history, which is a white noise (all frequency components are equally but randomly included), is modified by trials and errors until the frequency components satisfy the desired response spectrum (Fig. 5.26; see Sect. 23.1). The obtained time history is further modified so that it may satisfy the desired time envelope (Fig. 5.27).

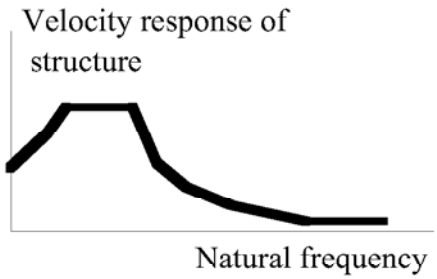

Fig. 5.26 Concept of response spectrum of design earthquake motion

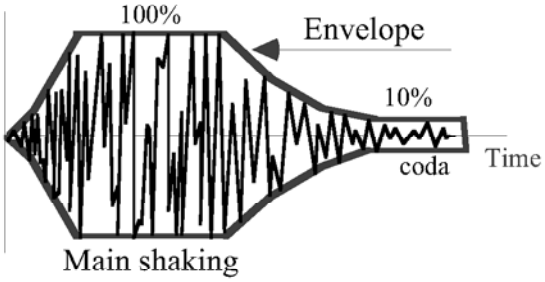

Fig. 5.27 Concept of time envelope of design earthquake motion

5.14 Seismic Damage in Traditional Houses

Figure 5.28 shows a damaged shape of a Japanese traditional wooden house during the 1995 Kobe earthquake. Since the top roof was heavy as a stabilization against storm winds, while walls and columns did not have sufficient lateral resistance, the house was easily destroyed by the quake. Figure 5.29 by Mononobe (1924) summarizes data on damage rate of Japanese houses during two earthquakes. It is seen that there is a good correlation between the damage rate and the maximum acceleration, which justifies the use of inertia force as a design earthquake load (Sect. 7.1). Note, however, that the acceleration in this figure is not the observed acceleration. It was assessed many years later by using damage reports.

Fig. 5.28 Damaged shape of Japanese traditional house in Kobe

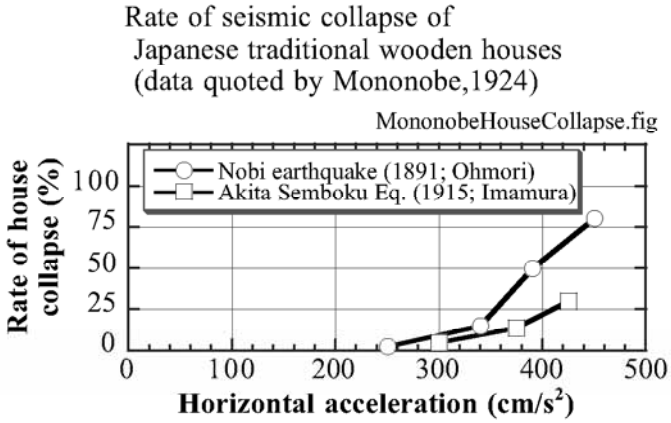

Fig. 5.29 Damage rate of Japanese traditional houses (Mononobe, 1924)

Fig. 5.30 Undamaged wooden house in Kobe (1995)

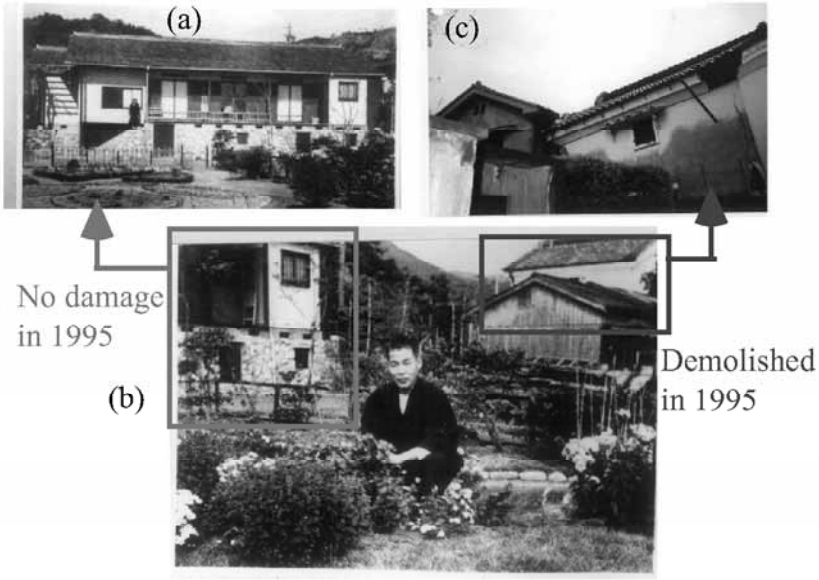

Fig. 5.31 Contrast in damage extent between soft wooden house and rigid ware house (1995 in Kobe; black-and-white photographs in 1948)

It may be pointed out that the damage rate is affected by local soil conditions. Figure 5.30 is a traditional house in Kobe as well which was not affected by the quake. Although the damage rate was low in the particular area of this house, a traditional ware house in the same area was significantly affected by horizontal shear failure near the bottom and was demolished. A traditional ware house is made of thick walls consisting of compacted earth (Fig. 5.31c) and wooden embedded reinforcement and it seems to have much greater shear rigidity than a wooden house. Figure 5.31b shows the same ware house to the right as well as another traditional wooden house on the left. In contrast to the heavily damaged ware house, the wooden house (Fig. 5.31a) was subject to very minor damage such as cracking in its earthen wall. This remarkable difference in damage extent may be attributed to structural difference because the distance between two structures was merely 30 m and the local soil condition together with the nature of input seismic motion was probably similar.

In spite of this rigidity, the ware house was damaged probably due to the following reasons.

- The area of Figs. 5.30 and 5.31 has a stiff soil condition, which is made of fluvial gravelly subsoil. Due to its rigidity, the natural period of the ground was short (Sect. 6.8). Hence, the shaking in this area had short predominant period of motion as well (resonance).
- The ware house was rigid and its natural period was short. Therefore, probably resonance and strong response occurred in the rigid ware house. In contrast, wooden houses are generally soft and their natural period is long. Therefore, resonance did not occurr. The natural period was further elongated by the heavy roof, which is made heavy in the particular region in order to avoid typhoon wind effects.

Therefore, soil-structure interaction in the sense of matching between natural periods of ground and structure deserves engineering attention. Figure 5.32 illustrates the different extents of damage rate of wooden houses in Tokyo. It is therein seen that more houses were damaged in the east part of Tokyo where soil consists of soft young alluvium where ponds, rice field, and swamps were predominant until recent times (Figure 5.33). Conversely, damage was less significant in the west where pleistocene or tertiary hilly topography was predominant. This indicates clearly the importance of local soil conditions in damage extent of the community.

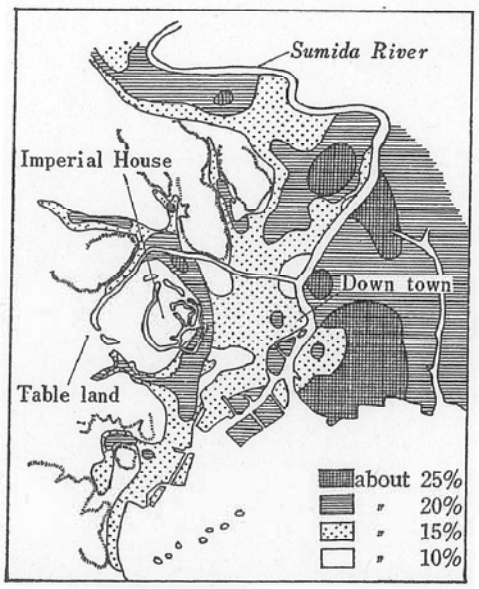

Fig. 5.32 Damage distribution of traditional wooden houses in Tokyo during 1923 Kanto earthquake (Okamoto, 1973)

For practical assessment of the natural period of a building, T, Japanese building engineers uses an empirical formula of

$$T(s) = H(0.02 + 0.01\alpha), \qquad (5.4)$$

in which H is the height of a building (meter) and α is the height ratio of floors in which columns and beams are made mainly of steel over the total building height. Housner (1961) proposed another formula of

$$T(s) = 0.1n, \qquad (5.5)$$

in which n stands for the number of storeys. For the natural period of ground, see (6.30).

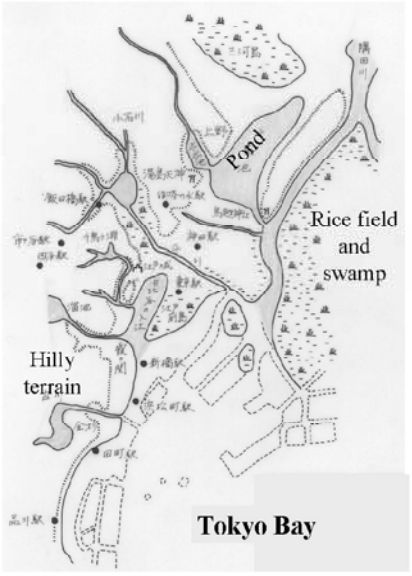

Fig. 5.33 Topography of Edo (present Tokyo) before AD 1600 (after Murai, 1994)

Matsuda et al. (1978) proposed an interesting idea on the basis of information about collapse rate of Japanese wooden houses (Fig. 5.28 for example) during the 1923 Kanto earthquake. The data was collected from Yokohama City and was compared with the thickness of alluvial soils as well as the natural period of the ground. The natural period was determined by running dynamic analyses with a complex modulus approach (Sect. 9.6) and detecting the period at which the amplification was maximum. Thus, the natural period corresponds to the resonance period.

Figure 5.34 shows the relationship between natural period of ground and the maximum amplification of earthquake motion. It is therein seen that the areas of greater collapse rate of houses had the longer natural period, approaching the natural period of houses. In contrast, the maximum amplification did not have much correlation with the collapse rate. Figure 5.35, moreover, indicates the relationship between the thickness of soft soil and the natural period of ground. It is seen that the area of higher collapse rate was associated with the greater thickness of soil and the longer natural period. Matsuda et al. (1978) consequently suggested that traditional houses were destroyed by strong response due to resonance and the amplification of seismic motion in the soil was less important. The importance of natural period of structures was already found in Fig. 5.31.

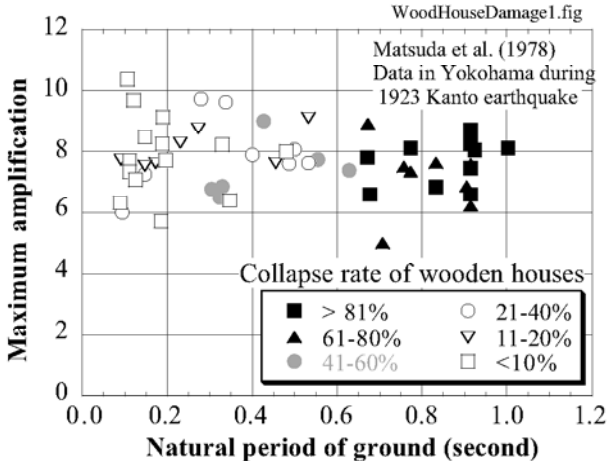

Fig. 5.34 Relationship between natural period of ground and maximum amplification changing with collapse rate of traditional wooden houses (Matsuda et al., 1978)

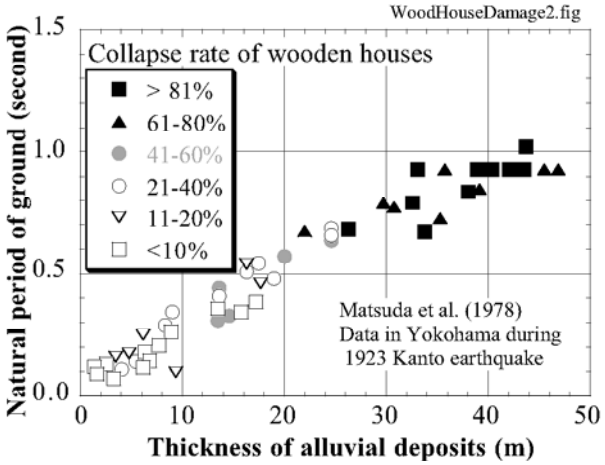

Fig. 5.35 Relationship between thickness of alluvium and natural period of ground changing with collapse rate of traditional wooden houses (Matsuda et al., 1978)

Fig. 5.36 Collapsed adobe house in Bam, Iran, in 2004

Fig. 5.37 Collapse of adobe house with heavy roof (Gilan, Iran, 1990)

Fig. 5.38 Heavy roof of traditional house in Kerman, Iran

Fig. 5.39 House of good maintenance which survived Bam earthquake in Iran

Traditional houses in Central Asia, which are made of masonry, have many problems as well. Figure 5.36 is the collapsed shape of a house that was made of adobe. Being a sun-baked brick, adobe can be easily made by using locally available materials and is widely used in arid countries. Since masonry walls made of adobe or other bricks cannot bear tensile force, bending failure is easy to occur, see Fig. 5.37.

The bending moment increases as the roof becomes heavier. Therefore, it may be desired to reduce the weight of the roof. However, local people tends to increase the weight by placing layers of bricks and mud. Consequently, many houses have very thick roofs (Fig. 5.38). This is because a heavy roof can avoid leakage of rain water and, together with thick walls, keep the inside temperature cool during hot daytime, while the stored sun heat maintains inside warm during cool night. Thus, seismic safety and daily convenience may conflict with each other. Note, however, that a house of good construction and maintenance in Bam (Fig. 5.39) was able to survive the devastating quake in 2004, and indicates the importance of the quality control in housing. The general principles in seismic safety of adobe or masonry houses are as what follows;

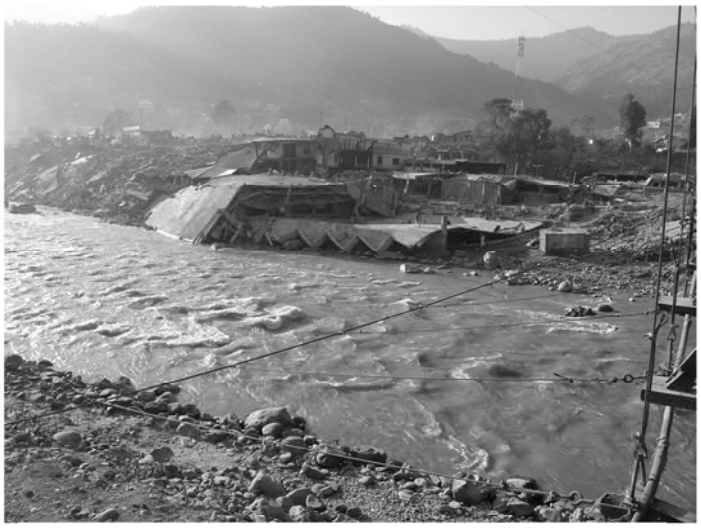

Fig. 5.40 Total collapse of buildings in Balakot, Pakistan, in 2005

- Daily convenience should be sacrificed to some extent for seismic safety.
- Cost of seismic retrofitting (improvement of earthquake safety) has to be low.
- Technology of seismic retrofitting of existing houses is still being sought for.
- Both retrofitting and new construction of earthquake-safe houses have to be achieved by using cheap locally-available materials.
- Since houses are constructed by local contractors, technology transfer for seismic safety should be done on a local basis by using languages that local people can understand.

One should not imagine from the discussion above that reinforced concrete buildings have less number of problems. Figure 5.40 shows the entire collapse of Balakot in Pakistan in 2005, which was induced by inappropriate seismic resistance of local buildings.

The importance of technology transfer is often discussed in international engineering and disaster-mitigation occasions. In the author´s opinion, highly educated engineers and designers in most countries in the world are doing good jobs. Engineered bridges and towers are able to survive strong earthquake motions. The real problem lies in the lack of technology transfer inside the country. In many countries, design codes and regulations are written in English because English is the common and official language when the nation is composed of many language groups. Although this idea is rational and lawful, many local contractors cannot read English documents. Moreover, the central government may not be able to control the quality of small constructions; codes are not respected. It therefore seems that domestic technology transfer is very important by publishing simplilfied translation / guidance of codes. Not only forcing contractors but also supplying incentives to contractors and customers is desired. Figure 5.39 showed that good quality of construction is able to improve the seismic resistance. Another issue is the maintenance. Decay of materials and dislocation of masonries reduces the seismic resistance. Again incentive to owners for better maintenance is needed.

Fig. 5.41 Tilting towards direction of no wall rigidity

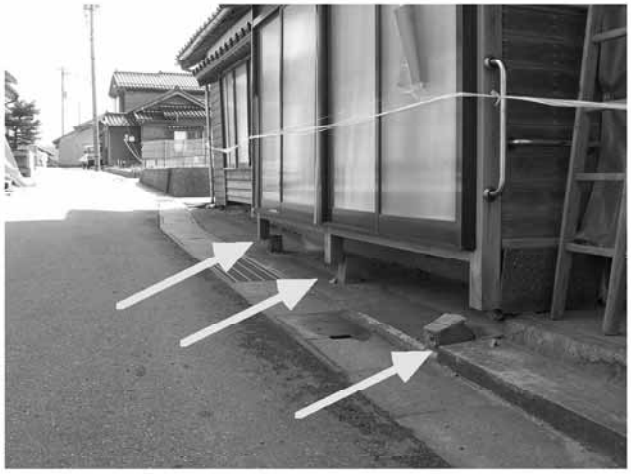

Fig. 5.42 Dislocation of house from foundation

The problem of wall is important as well in Japanese traditional houses. Figure 5.41 shows a totally destroyed house in Douge of Wajima City (輪島市門前 道下地区) during the 2007 Noto earthquake. Significant tilting towards the direction without wall resistance is evident. Figure 5.42 reveals the problem of traditional foundation. Since the super structure was simply resting on small stones without mechanical connection, the strong inertia force (horizontal acceleration being more than 900 Gal probably) easily made the house separated from the foundation.

🕮 5.15 Reconnaissance Study of Earthquake-Induced Damage

This section is intended to supply some useful knowledge about damage investigation after a severe earthquake event. The special attention is focused on an international damage investigation out of one's home country.

1. Good health

All the efforts should be done to avoid local diseases, which one is not used to. It is a must to have preventive shot against tetanus, which comes from contaminated soils and might be fatal. A disinfectant should be always carried at hand. Rabies or hydrophobia is another important disease in some countries. Care should be taken of food poisoning. A very strong binding medicine is useful, if no bacteria is involved. However, a suitable antibiotic medicine should be prepared to stop diarrhea caused by bacteria. A good medical doctor is not always available in most parts of the world.

It is certainly important during a trip not to take suspicious food and drink. While food cooked by heat is mostly safe, raw food and those washed by tap water often cause troubles. Safe foods are such as baked meat and boiled food. Hot tea (called "*gyarm chai*" in Iran and Pakistan) as well as yogurt are generally safe and good. Banana is an ideal lunch because it is cheap and its inside is perfectly clean (Fig. 5.43). Recently, safe mineral water is supplied in bottles almost everywhere. To be more confident, however, bottled mineral water containing CO_2 gas ("*agua mineral con gas*") is recommended. On the other hand, many people have bad stomach problems caused by cut fruits, fresh salad, and iced drinks. Local spicy food often causes diarrhea because your stomach is not used to it. It is advisable, therefore, to carry a role of toilet paper for an unexpected emergency situation.

Fig. 5.43 Shopping banana in local market (Mansehra in Pakistan) (Abbotabad, Pakistan)

Fig. 5.44 Ruin of building which collapsed suddenly upon minor aftershock

In addition to diseases, Fig. 5.44 shows a building in Abbotabad of Pakistan. This building was already damaged during an earthquake on October 8th, 2005, but managed to stand for more than one month. In the morning of November 20th, there was a minor aftershock, and this building suddenly collapsed as shown in the photograph. If anybody had entered this building at that moment for damage investigation, the situation could have been fatal. Another risk in a collapsed building is the nails in pieces of wooden walls and columns. To avoid injury due to walking upon nails, safety boots with steel plates inside are highly recommendable. Thus, entering damaged structures and buildings should be made very carefully on one´s own risk. The author also experienced flooding of river in the center of a dry desert in Iran. Thus, one has to be prepared for a totally unexpected situation.

2. What should be brought

A topographical map of the affected area is very important. Your local counterpart researcher may prepare a detailed map. If it is not possible or if the local government does not publish a good map due to military reasons, air pilot's maps that are of the scale of 1:500,000 and are prepared by the Defense Mapping Agency Aerospace Center, St. Louis, Missouri, are available in major bookstores. Moreover, the exact location can be identified by a GPS equipment in any part of the world.

Taking pictures is absolutely important. The importance of pictures, however, deteriorates quickly after the excursion, because many researchers take similar photographs and people become familiar with them. It is important to take pictures that would support one's interpretation (theory) of the damage mechanism. Hence, some pictures should be taken of with some scenario in your mind. Note that a good photograph chance comes only one time during the trip and not twice. Therefore, do not postpone the chance until the next time.

It is essential to collect data/information other than photographs. Example data may be the size of a landslide mass, the width of ground cracks, the extent of ground movement, and damage distribution correlated with local geology. A local publication such as design code is important as well. Photographs of a damaged site prior to the quake may be found in a tourist book, which is available in a local bookstore. Moreover, subsoil investigation is possible by a portable cone penetrometer in clayey ground and a Swedish weight sounding in a loose sandy ground (Sect. 8.9). The equipment in Fig. 5.45 (developed by Dr. Sakai, the Kisojiban Consultants Inc., Tokyo) employs local soil as the 100- kg weight in place of metal weights so that the necessary equipments can be transported. In Fig. 5.44, sand is put in blue plastic bags which are hanging on the equipment.

Fig. 5.45 Subsurface investigation by Swedish weight sounding supervised by Dr. Ilyas Suratman of Bandung Institute of Technology (Banda Aceh in Sumatra, Indonesia)

Although collecting samples of geomaterials for laboratory tests is important, quarantine regulations should be respected. Moreover, different practices in standard penetration tests and their effects on blow counts should be borne in mind, if boring profile is obtained.

3. Collaboration with local counterparts and people

International investigation is made easier and safer if one can work with local engineers and/or researchers. This is because they can make a detailed and reasonable travel plan and arrange transportations (4-wheel-drive vehicle is desirable) as well as accommodations. No complaint should be made to a possibly humble accommodation because the present trip is not sight-seeing. Moreover, those people may be able to obtain useful information. For example, inquiry to earthquake-affected people is made possible through their language-interpretation. To appreciate their collaboration, one should pay their travel expenses. It is another good idea to visit the counterpart's institution at the end of the trip in order to report and discuss about research findings. Coauthoring and submitting a report paper in an international journal is a very good idea.

The trip is made easier by learning a local language. Saying only "hello" and "thank you" with local

people improves the situation significantly. It should not be insisted that English is an international language and that everybody should understand it. Such an idea never makes sense. See Appendix 2.

List of References in Chapter 5

Arangelovski, G. and Towhata, I. (2004) Accumulated deformation of sand with initial shear stress and effective stress state lying near failure conditions, Soils and Foundations, Vol. 44, No. 6, pp. 1–16.

Arias, A. (1970) A measure of earthquake intensity, Seismic Design for Nuclear Power Plants, Hansen, R.J. Ed., MIT Press, pp. 438–483.

Gutenberg, B. (1945a) Amplitude of surface waves and magnitudes of shallow earthquakes, Bull. SeismoL. Soc. Am., Vol. 35, pp. 3–12.

Gutenberg, B. (1945b) Amplitude of P, PP and magnitude of shallow earthquakes, Bull. SeismoL. Soc. Am., Vol. 35, pp. 57–69.

Gutenberg, B. (1945c) Magnitude determination for deep-focus earthquakes, Bull. SeismoL. Soc. Am., Vol. 35, pp. 117–130.

Housner, G. W. (1961) Vibration of structures induced by seismic waves, Part I. Earthquakes, Shock and Vibration Handbook, Harris, C.M. and Crede, C.E. Ed., McGraw-Hill, New York, pp. 50-1–50-32.

Housner, G.W. (1965) Intensity of earthquake ground shaking near the causative fault, Proc. 3rd World Conf. Earthq. Eng., Vol. 1, pp. III-94–III-115.

Irikura, K. (1983) Semi-empirical estimation of strong ground motions during large earthquakes, Bull. Disaster Prevention Res. Inst., Kyoto University, pp. 63–104.

Irikura, K. (1986) Prediction of strong acceleration motion using empirical Green's function, 7th Japan Earthq. Eng. Symp., pp. 151–156.

Joyner, W.B. and Boore, D.M. (1996) Recent developments in strong-motion attenuation relationships, Proc. UJNR 28th Joint Meeting of United States-Japan Panel on Wind and Seismic Effects, NIST SP 904, Gaithersburg, pp. 101–115.

Kanai, K. and Suzuki, T. (1968) Expectancy of the maximum velocity amplitude of earthquake ground motions at bedrock, Bull. Earthq. Res. Inst., University of Tokyo, Vol. 46, pp. 663–666.

Kawashima, K., Aizawa, K. and Takahashi, K. (1985) Duration of strong motion acceleration records, Proc. JSCE, Struct. Eng. Earthq. Eng., Vol. 2, No. 2, pp.161–168

Kawasumi, H. (1951) Measures of earthquake danger and expectancy of maximum intensity throughout Japan as Inferred from the seismic activity, Bull. Earthq. Res. Inst., University of Tokyo, Vol. 29, pp. 469–482.

Kobayashi, H. and Midorikawa, S. (1982) A semi-empirical method for estimating response spectra of near-field ground motions with regard to fault rupture, Proc. 7th Eur. Conf. Earthq. Eng., Vol. 2, pp. 161–168.

Lee, K.L. and Chan, K. (1972) Number of equivalent significant cycles in strong motion earthquakes, Proc. Int. Conf. Microzonation Safer Construct. Res. Appl., pp. 609–627.

Matsuda, I., Wada, S. and Miyano, M. (1978) The relation between subsoil condition and the collapse rate of wooden houses due to the Great Kanto earthquake of 1923 in Yokohama City, J. Geography, Tokyo Geographical Society, Vol. 87, No. 5, pp. 14–23 (in Japanese).

Mendoza, M.J. and Romo, M.P. (1998) Performance of a friction pile-box foundation in Mexico City clay, Soils Found., Vol. 38, No. 4, pp. 239–249.

Meteorological Agency (1968) Guideline for earthquake observation, Appendix for reference information, p. 78 (in Japanese).

Mononobe, N. (1924) Discussion and consideration on vertical earthquake motion and consideration, Proc. JSCE, Vol. 10, No. 5, pp. 1063–1095 (in Japanese).

Murai, M. (1994) Edo castle and life of shogun family, Chuko Shinsho, No. 45, P. 5 (in Japanese).

Okada, S., Orense, R., Kasahara, Y. and Towhata, I. (1999) Prediction of liquefaction-induced deformations of river embankments, Proc. Second Int. Conf. Earthq. Geotech. Eng., Vol. 2, pp. 543–548.

Okamoto, S. (1973) Introduction of earthquake engineering, University of Tokyo Press, p. 62.
Richter, C.F. (1935) An instrumental magnitude scale, Bull. SeismL. Soc. Am., Vol. 25, pp. 1–32.
Seed, R.B., Dickenson, S.E. and Idriss, I.M. (1991) Principal geotechnical aspects of the 1989 Loma Prieta earthquake, Soils Found., Vol. 31, No. 1, pp. 1–26.
Tamura, C., Hakuno, M., Abe, K., Iemura, H., Katada, T. and Takeuchi, M. (1987) Report on Mexico earthquake September 19, 1985, Nuclear Power Department, Report 006, Okumura Corporation (in Japanese).
Utsu, T. 宇津徳治 (1999) 地震活動総説 Seismic studies: a comprehensive review, University of Tokyo Press, 東京大学出版会, ISBN 4-13-060728-6 (in Japanese).